Controls and timing of Cenomanian-Turonian organic enrichment andrelationship to the OAE2 event in Morocco, North Africa

Jianpeng Wang, Luc G. Bulot, Kevin G. Taylor, Jonathan Redfern

Journal Pre-proof

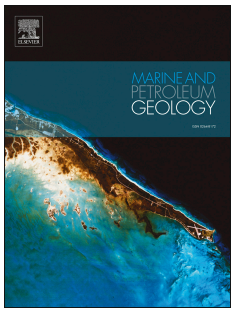

For Marine and Petroleum geology Controls and timing of Cenomanian-Turonian organic enrichment and relationship to the OAE2 event in Morocco, North Africa

Jianpeng Wang, Luc G. Bulot, Kevin G. Taylor, Jonathan Redfern

PII: S0264-8172(21)00116-1

DOI: https://doi.org/10.1016/j.marpetgeo.2021.105013

Reference: JMPG 105013

To appear in: *Marine and Petroleum Geology*

Received Date: 26 September 2019

Revised Date: 13 November 2020

Accepted Date: 28 February 2021

Please cite this article as: Wang, J., Bulot, L.G., Taylor, K.G., Redfern, J., For Marine and Petroleum geology Controls and timing of Cenomanian-Turonian organic enrichment and relationship to the OAE2 event in Morocco, North Africa *Marine and Petroleum Geology*, https://doi.org/10.1016/j.marpetgeo.2021.105013.

Jianpeng Wang: Conceptualization, Methodology, Fieldwork, experiment, data analysis, Writing- Original draft preparation

Luc G. Bulot: Stratigraphy analysis, fieldwork, Reviewing and Editing

Kevin Taylor: Geochemical analysis, Reviewing and Editing

Jonathan Redferen: Field work, Sedimentology analysis, Reviewing and Editing

For Marine and Petroleum geology

Controls and timing of Cenomanian-Turonian organic enrichment and relationship to the OAE2 event in Morocco, North Africa

Jianpeng Wang[1], Luc G. Bulot[2,1], Kevin G. Taylor[1] , Jonathan Redfern[1]

[1] North Africa Research Group, Department of Earth and Environmental Sciences, University of Manchester, Manchester, M13 9PL, UK.

[2] Aix-Marseille Université, CNRS, INRD, IRA, Collège de France, CEREGE, France

Abstract

The Cenomanian-Turonian Oceanic Anoxic Event (OAE2) is a significant global event that has been linked to major source rock development in marine environments. The aim of this study is to integrate biostratigraphic, sedimentological and geochemical data (including stable carbon isotopes and trace elements) to document the timing and controls of organic matter enrichment across the Cenomanian-Turonian boundary.

Morocco has excellent exposures of Tethyan carbonate platform and basinal facies and this paper details a high-resolution analysis of organic-rich Late Cretaceous intervals exposed in the Errachidia-Goulmima Basin, to investigate their relationship to the OAE2. Integrating planktic foraminiferal and ammonite biostratigraphy with carbon isotope correlations indicate that organic-rich black mudstones identified were deposited from latest Cenomanian to early Turonian, suggesting a late-OAE2 to post-OAE2 age.

The sedimentology, redox water conditions and palaeoproductivity of the palaeoenvironments were studied to characterise the lithofacies and geochemical signatures, and to analyse the controlling factors for organic–enrichment. In the study area during the

lower OAE2 interval, a shallow water mid-ramp environment prevailed, with predominantly bivalve-rich limestone deposition. Subsequent organic-rich mudstone development can be correlated with the latest Cenomanian (late OAE2 interval) and early Turonian (post-OAE interval) transgression, which allowed development of anoxic to euxinic conditions in the outer-ramp environment, characterized by high TOC values, from 2.7 to 17 wt%. Shallow platform locations continued to experience limestone deposition with no organic enrichment.

Trace and major element data from the C/T black mudstones show an extremely high concentration in palaeoproductivity-sensitive (P, Zn, Ni and Cu) and redox-sensitive elements (V, Mo, and U). The redox environments evolved from dysoxia to anoxia and sulfidic euxinia, which is interpreted to have provided optimum conditions for organic carbon preservation in the Errachidia area.

The results highlight the important interplay of local paleogeography and eustatic sea-level (the late Cenomanian/early Turonian transgressions) as the main controls on organic mudstone deposition, rather than simply global OAE2 control. The development of organic-rich mudstones reflects both increased productivity at this time and enhanced organic matter preservation due to the change in redox bottom water conditions.

Keywords: Cenomanian, Turonian, OAE2, Organic carbon, Carbonate platform, Stratigraphy, Geochemistry, Morocco

1. Introduction

The Cenomanian-Turonian Oceanic Anoxic Event (OAE2) was a significant global event that has been linked to the widespread deposition of organic carbon in a variety of palaeobathymetric settings, such as continental margins, shelf seas and abyssal plains (Schlanger and Jenkyns, 1976; Schlanger et al., 1987; Kolonic et al., 2005). These

approximately coeval stratigraphic deposition of global organic-rich mudstones in the late Cenomanian and early Turonian (C/T) intervals have been extensively studied, but there is still debate on the local to global controls on the deposition of enhanced organic matter (OM) accumulations and its relation to the OAE2 (Schlanger et al., 1987; Sageman et al., 2003; Lüning et al., 2004; Kolonic et al., 2005; Brumsack, 2006; Jarvis et al., 2011; Jarvis et al., 2015).

The OAE2 has been extensively studied in deep-water basins, where well-preserved OM-rich black mudstones and shales have been reported, and can be correlated to a positive carbon isotope excursion (Tsikos et al., 2004; Kolonic et al., 2005; Kuhnt et al., 2017). However, C/T OM-rich mudstones were only rarely developed in shallow carbonate platforms, despite the strata recording the typical $\delta^{13}C$ positive excursion of the OAE2 interval (Elrick et al., 2009; Gertsch et al., 2010; El-Sabbagh et al., 2011; Korbar et al., 2012). A number of questions remain regarding the controls of OM accumulation and the response of the OAE2 in shallow marine settings.

A wide shallow carbonate platform developed across the West Saharan platform during the Late Cenomanian to Early Turonian (Benadla et al., 2018), and outcrops in the Pre-African basins of Morocco afford the opportunity to address some of these outstanding questions.

The Upper Cenomanian to Lower Turonian successions in the Errachidia-Goulmima Basin are dominated by shallow-marine palaeoenvironments (Lézin et al., 2012). These deposits contain comparable fossil assemblages and facies to paleo-Tethys Ocean-influenced platform sediments across Tunisia and Algeria (Caron et al., 2006; Grosheny et al., 2008; Zagrarni et al., 2008; Reolid et al., 2015; Aguado et al., 2016; Ferré et al., 2017; Benadla et al., 2018). In the Errachidia-Goulmima Basin, the interval has been the focus of a number of previous biostratigraphic studies, based on ammonites (Kennedy et al., 2008; Meister et al., 2017),

planktic foraminifera (Lézin et al., 2012; Reolid et al., 2015) and ostracods (Andreu et al., 2013; Benadla et al., 2018). Lézin et al. (2012) integrated biostratigraphic data with a $\delta^{13}C$ study, but the results were inconclusive and several possible locations for the C/T boundary were proposed. The uncertain position of the C/T boundary in this area has impeded regional and global correlation, and thus further assessment of global paleoclimate change or the relationship of eustatic sea level change to the deposition of C/T strata. Lézin et al. (2013) also undertook the first geochemical analysis on samples in the studied basin, including at the Goulmima and Ziz sections, proposing an oxygenated water condition in the Upper Cenomanian, but a reducing condition recorded in the Lower Turonian induced by the increased palaeoproducitivity related to geochemical weathering input. However, they did not identify any sections with anoxic bottom water conditions or organic-rich sediments, and as such were unable to evaluate any association of anoxia and organic carbon burial to the OAE2 in this area.

This paper presents detailed sedimentological, palaeontological, mineralogical and geochemical analyses undertaken on seven sections in the Pre-African Trough, focusing on the Errachidia-Goulmima Basin. The purpose of this study is firstly to describe the distribution and characteristics of organic carbon in this shallow marine carbonate platform environment, and secondly to build a new C/T stratigraphic framework to improve regional correlation to the C/T boundary and OAE2. Thirdly, this study reconstructs the palaeoenvironment of the Tethyan Errachidia-Goulmima Basin and investigates the driving factors for organic matter sequestration and black shale deposition in order to better understand the OAE2 response in shallow platform environments.

2. Geological setting

Located in southeast Morocco, the Pre-African Trough extends over the provinces of Souss-

Massa-Drâa and Meknes-Tafilalet. It forms a low-relief plain, sandwiched between the Moroccan High Atlas to the North and the Anti-Atlas mountain range to the South (Figure 1). From west to east, the Pre-African Trough can be subdivided into the Souss, Ouarzazate and Errachidia-Boudnib-Erfoud Basins(Ambroggi and Choubert, 1952).

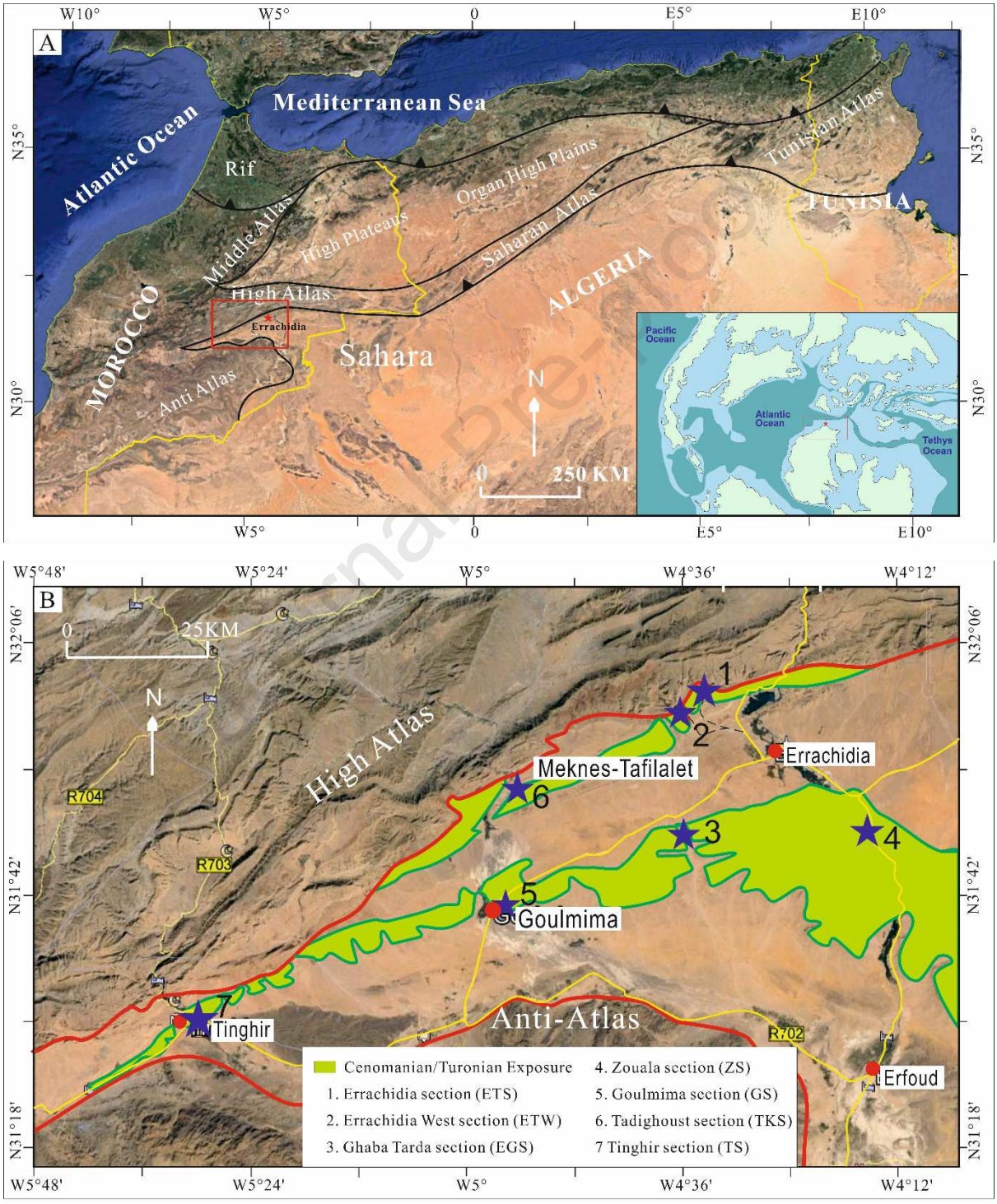

Figure 1. Location of studied sections in the Errachidia-Goulmima Basin. The late Cenomanian-early Turonian palaeogeography (inset Fig 1A) of Northwest Africa (modified after Weaver et al., 2000)

The Cretaceous succession lies unconformably upon either Palaeozoic or Jurassic sediments. It is dominated by shallow-marine palaeoenvironments comprising similar facies and fossil assemblages to Neo-Tethys platform deposits described from Algeria and Tunisia (Busson et al., 1999; Grosheny et al., 2008; Zagrarni et al., 2008; Robaszynski et al., 2010; Grosheny et al., 2013; Reolid et al., 2015; Benyoucef et al., 2016; Benyoucef et al., 2017; Benadla et al., 2018). The absence of Cretaceous strata in most of the High Atlas and Anti Atlas is attributed to post-Cretaceous erosion. It is likely that Cenomanian/Turonian deposition extended across a large part of these areas, with maximum depositional extent during the early Turonian transgression(Zouhri et al., 2008).

Seven outcrops were studied in the Errachidia-Goulmima Basin: 1. the Errachidia section (Errachidia) (lat 31°59'53"N and long 4°33'29"W), 2. the Errachidia West section (ETW) (lat 31°59'5"N and long 4°34'57"W), 3. the Ghaba Tarda section (EGS) (lat 31°48'50"N and long 4°36'7"W), 4. the Zouala section (ZS) (lat 31°48'1"N and long 4°14'17"W), 5.the Goulmima Section (GS) (lat 31°42'30"N and long 4°55'43"W), 6. the Tadighoust section (TKS) (lat 31°52'22"N and long 4°55'56"W) and 7. the Tinghir section (TS) (lat 31°31'57"N and long 5°28'33"W) (Fig. 1B).

These sections belong to the Cenomanian–Turonian Akrabou Formation, which was introduced by Dubar (1948) (Dubar, 1948), and formally defined by Ettachfini and Andreu (2004) (Figure 2). The thickness of the Akrabou Fm. varies from 12m to 50 m across the basin. It is subdivided into four lithostratigraphic units (Unit C1, C2, T1 and T2), that are bound by regional unconformities (D2 to D6) (Ettachfini and Andreu, 2004) (Figure 2). Lateral facies changes were recognised and extensively discussed by Ettachfini and Andreu (2004). The biostratigraphic interpretation of the successions was initially based on ammonites, foraminifera and ostracods, and the C/T boundary was tentatively placed at the

base of unit T1 and marked by a major regional unconformity (D4) (Ettachfini and Andreu, 2004; Lézin et al., 2012; Andreu et al., 2013). The T1 and T2 units were defined at the ammonite rich section of Tadighoust (Kennedy et al., 2008).

This scheme was modified in subsequent work by Lézin et al. (2012), Andreu et al. (2013) and Lebedel et al. (2013), following collection of new data (ammonites, foraminifera and $\delta^{13}C$). The Upper Cenomanian to Lower Turonian age of the formation was confirmed, but the C/T boundary was shifted to a position equivalent to the D5 unconformity of Ettachfini and Andreu (2004) (Figure 2).

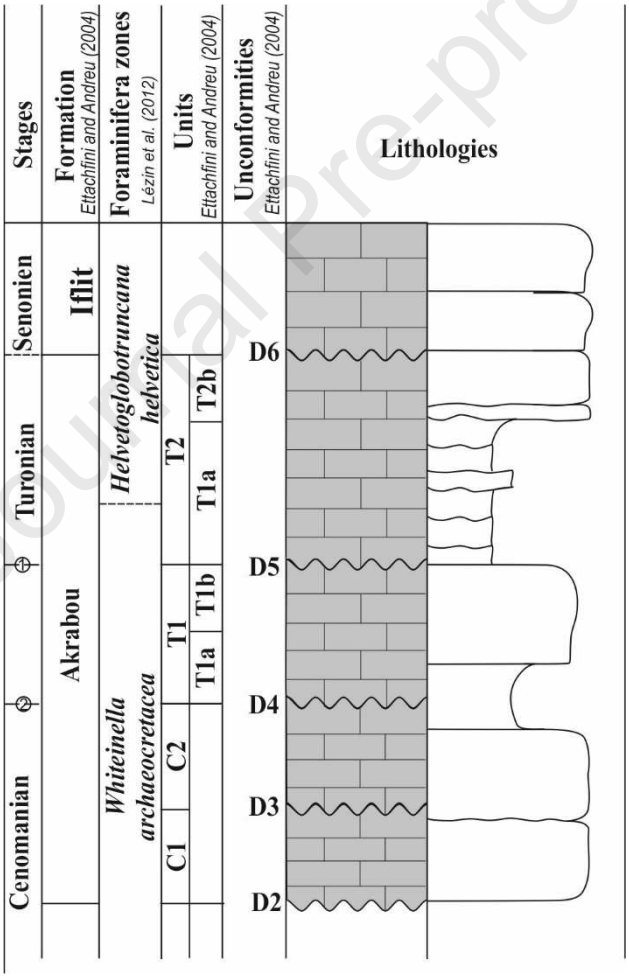

Figure 2. Stratigraphic column and unconformities in Pre-African basin. The position of Cenomanian/Turonian boundary as it was previously defined by (a) Lézin et al. (2012) and (b) Ettachfini and Andreu (2004).

3. Materials and Methods

A total of seven sections were logged at high resolution and photographed, and 268 samples of limestones, marls and organic-rich mudrocks collected to investigate the palaeoenvironmental changes during the C/T transition. A number of samples (102 in total) from the Errachidia, Goulmima and Tadighoust sections were made into thin sections and polished for optical and scanning electron microscopy observation.

A total of 52 samples were selected for XRF analysis. These were made into pressed pellet-shape samples and analysed using Axios Sequential X-ray Fluorescence Spectrometer at the University of Manchester. The obtained trace elements were normalized to aluminium to eliminate the dilution effect of detrital input linked to silicates (Turekian and Wedepohl, 1961; Wedepohl, 1971; Brumsack, 1989; Calvert and Pedersen, 1993; Wedepohl, 1995). All the trace elements are displayed as Al-normalized values with units of 10^{-4}. The richness of elements is expressed as normalized elements divided by average shale (As) values (Brumsack, 1989, 2006), using the average shale compositions of Wedepohl (1971). Enrichment factors (EFs) were calculated using:

$$\mathbf{EF_{element} = (element/Al)_{sample} / (element/Al)_{As}}$$

Using the enrichment factors, five categories, based on the work of Sutherland (2000), were used to describe enrichment in the sediments: 1) EF<2, depleted concentration; 2) 2<EF<5, moderate enrichment; 3) 5<EF<20, significant enrichment; 4) 20<EF<40 highly enriched elements; 5) EF>40, extremely enriched elements.

Carbon and oxygen stable isotope analysis ($\delta^{13}C$ and $\delta^{18}O$) on samples from the Errachidia section were carried out at the University of Liverpool using an Elemental Analyser coupled to the Thermo Scientific Delta VAdvantage mass spectrometer fitted with Conflo IV gas handling system, with the purpose of identifying the OAE2 interval and C/T boundary based

on correlation to published regional and global $\delta^{13}C$ curves. Small amounts (a few grams) of samples were carefully selected from the fresh samples collected in the field. All samples were pre-treated in order to remove reactive organic compounds present in bulk limestones prior to isotopic analysis. The carbon ($^{13}C/^{12}C$) and oxygen ($^{18}O/^{16}O$) isotope ratios of bulk limestone samples were measured following a modified version of the classical manual 'sealed vessel' procedure described by McCrea (1950) and Swart et al. (1991) (McCrea, 1950; Swart et al., 1991). Data are reported as delta (δ) values with respect to the Vienna Pee Dee Belemnite (VPDB) carbon and oxygen isotope scales (*via* NBS 19, NBS 18). Analytical precision (1σ), based on replicate analysis of inhouse quality control calcite, is estimated to be ±0.04 ‰ for carbon isotope values and ±0.06 ‰ for oxygen isotope values. Mineralogical quantification was performed on 51 samples from the Errachidia section using a Philips PW1730 and Bruker D8 Advance in the University of Manchester, to identify the compositions of organic-poor limestones and organic-rich mudstones. A total of 35 samples have been analysed for Total Organic Carbon content (TOC) from the Errachidia section, using a Leco carbon analyser in the University of Manchester and Jilin University. The TOC values were calculated by subtracting the Inorganic Carbon (IC) values from the Total Carbon (TC) values.

4 Sedimentology and Results

4.1. **Lithofacies**

Twelve lithofacies are identified from the seven studied sections, based on sedimentological features and fossil assemblages, detailed on Table 1.

These lithofacies can be grouped into three broad associations:

185 **Fossil-rich packstone-floatstone** (LF1-LF7): widely developed in the lower part of the
186 sections (Figure 3 and Figure 4), displaying deposition on a generally shallow carbonate
187 marine platform, midramp to inner-ramp environment.

188 **Fine-grained wackestone or black mudrock** (LF8-LF10) dominates the middle part of the
189 section (Figure 5), intercalated with bivalve-rich grainstone, showing a dominant deeper
190 outer-ramp marine deposition.

191 **Bivalve rich floatstone** (LF11 and LF12) forms the upper part of most logged sections
192 (Figure 5), presenting a mid-ramp environment again.

193 Based on the above lithological patterns and fossil assemblages, a regional correlation was
194 carried out (Figure 6) and three depositional units were defined: a lower bioclastic limestone
195 unit (LBL), a middle fine-grained limestone unit (MFL) and an upper bioclastic limestone
196 (UBL) unit (Figure 6 and Table 1).

197 **4.1.1. Lower Bioclastic Limestone (LBL) Unit**

198 This unit forms the basal part of the Cenomanian-Turonian deposition in this area, it is the
199 thickest unit and is dominated by fossil-rich limestone (from wackestone to floatstone).
200 These strata contain abundant benthic fauna (bivalves, gastropods, echinoids, benthic
201 foraminifera and ostracods) and associated minor planktic fauna (planktic foraminifera and
202 calcispheres). Seven lithofacies were identified in this unit (Table 1).

203 LF1 and LF2 are the two most common lithofacies in this unit. Beds are relatively thick, up
204 to 2 m in the lower part of the Errachidia section. Also common are nodular, thin-bedded
205 layers (less than 20cm) interbedded with thin marly limestone. These are widely observed in
206 all sections except the Zouala section (Figure 1B and Figure 6). LF3 and LF 4 are also well
207 developed in this unit, mainly distributed towards the middle part (the Errachidia, Tadighoust

and Goulmima sections). The unit is dominated by a diverse assemblage of small macrofossils, such as bivalves, gastropods and some shell fragments, together with ostracods and foraminifera microfossils. LF5 is only identified in the Zouala section, and is characterized by a floatstone dominated by large *Nerinea* (gastropods). LF6 and LF7 are also locally recorded in the Zouala and Ghaba Tarda sections in this unit, with some beds comprising interbeds of these two lithofacies (Figure 6).

The high amount of micrite matrix and the presence of well-preserved fossils in LF1 and LF2 suggest a low energy environment below the fair weather wave base (FWWB). The co-occurrence of large bivalves/oyster fragments with a micrite matrix could be evidence of reworking by strong wave action and redeposited in a relative quite condition between the FWWB and the storm wave base (SWB), suggesting a mid-ramp environment. The abundant reworked shell fragments in LF3 and LF4 are interpreted to be a medium-energy environment above the SWB, and integrated with rarely developed benthic foraminifera, suggesting a mid-ramp environment. LF5 was commonly developed in between the lower part of the intertidal zone to the upper subtidal zone (HUA□ZHANG, 1990), an inner ramp environment above FWWB. The abundance of rudist and reworked rudist fragments in the LF6 and LF7 indicate an inner-ramp setting. Overall, this unit is composed of a lithofacies association of mid- and inner-ramp conditions in the Zouala and Ghaba Tarda sections, while the other sections show deposition in a mid-ramp environment.

4.1.2. Middle Fine-Grained Limestone (MFL) Unit

This unit is composed of four lithofacies (Figure 4). Micritic limestones and mudstone (LF8/LF9) at the base, followed by bioclastic-rich limestone beds (LF2/LF10), and capped again by LF8/LF9. The foraminiferal wackestone lithofacies (LF 9) is the most commonly developed in all of the sections.

Organic-rich black mudrocks (LF8) were recorded in this unit in both the Errachidia and Errachidia West sections, interbedded with the OM-poor fine-grain limestone (LF9). The middle part of this unit is dominated in most of the studied area by LF10, consisting of nodular limestone beds that contain well-preserved bivalves. Individual beds are typically thinner than 20cm. However, in the Zouala and Ghaba Tarda sections, the middle part of this unit is mainly composed of LF2.

238 **Table 1 Characteristics and interpretations of lithofacies in the studied basin**

Lithofacies	Sedimentological features	Biogenic features	Interpretation	Sections	Unit
LF1 Oyster-rich floatstone (Figure 3 A)	Limestone with oyster beds interbedded with thin greyish fine-grain limestone or grey marls beds. Up to 2 m thick. Massive oysters distributed in a micrite limestone matrix.	Abundant large (up 10 cm) and well-preserved oysters (Figure 3 A1), some shell fragments (Figure 3 A2) and rare planktic and benthic foraminifera	Mid-ramp, low energy, above the SWB	ETS, ETW, GS, EGS, TKS, ZS and TS	LBL
LF2 Bivalve-rich floatstone (Figure 3 B)	Greyish bivalve-rich limestone, interbedded with thinly marly limestone or marls beds. Abundant bivalves distributed in a micrite matrix.	Abundant well-preserved bivalves (Figure 3 B1), bivalve fragments (Figure 3 B2), various size of bivalves up to 3cm		ETS, ETW, GS, EGS, TKS and TS	LBL MBL
LF3 Shelly wackestone	Thin beds of greyish wackestone interbedded with thin beds of marly limestone (Figure 3 C1).	Minor planktic and benthic foraminifera, and shell fragments (Figure 3 C2).	Middle ramp, low-medium energy, between the SWB and FWWB	ETS, ETW, GS, EGS, TKS and TS	LBL
LF4 Bivalve-rich packstone/grainstone	Greyish fossil-rich limestone interbedded with thin beds of marly limestone.	Abundant reworked bivalve shells, gastropods (Figure 3A1), ostracods, peloids, rare planktic foraminifera (Figure 3 D2)			
LF5 Gastropod-rich floatstone	Thick beds (up to 5m) of greyish micritic limestone with common gastropods (Figure 4 A).	Large Nerinea-dominated gastropods up to 10 cm long	Inner Ramp (above FWWB)	ZS	
LF6 Bryozoans-rich floatstone	Greyish bryozoans rich floatstone, up to 6 metres,	Abundant bryozoans (Figure 4B), commonly mixed with rudists, rare bivalves, echinoids fragments, benthic foraminifera.		ZS and EGS	

239

240

LF7 Rudistic floatstone	Yellowish thick rudist-rich floastone, rudist shells isotlated in a bioclastic wackestonepackstone matrix.	High abundance of Slightly reworked rudist shells and fragments (C1 and C2), and burrows and some bioclasts were identified in the mud matrix.	Inner Ramp (above FWWB)	ZS and EGS	
LF8 OM-rich black mudrock	Laminated black mudstone. Light grey to tan coloured when weathered, but black on freshly broken surfaces. (Figure 4 D3). Contains scattered calcite nodules (Figure 4 D1)	Abundant foraminifera (*Heterohelix* and *Whitenella*) (Figure 4 D2 and D4), some crinoids and rare oyster fragments (Figure 4 D4). No benthic foraminifera identified	Outer ramp below SWB	ETS and ETW	MFL
LF9 Foraminiferal-rich wackestone	Whitish and greyish limestone wakestone with intercalated carbonate nodules (Figure 5 A1), and carbonate layers	Abundant planktic foraminifera, and presence of crinoid and oyster fragments (Figure 5 A2)		ETS, ETW, GS, EGS, TKS, ZS and TS	
LF10 Nodular floatstone	Alternating thinly bedded nodular limestone and marly limestone (Figure 5 B1). Nodular limestone contains large bivalves.	Abundant well-preserved bivalves observed in the nodular limestone, abundant peloids and minor benthic foraminifera and ostracods (Figure 5 B2).	Middle Ramp, below the FWWB	ETS, ETW, GS and TKS	
LF11 Bivalve and crinoid-rich floatstone	Thick bedded (up to 80 cm) greyish grainstone with thickness (Figure 5 C1)	Well-preserved bivalves, shell fragments, crinoids and peloids were highly developed (Figure 5 C2)		ETS, ETW, and TKS	UBL
LF12 Bivalve and peloidal floatstone	Big package of grainstone some fossils are highly weathered (Figure 5 D1)	Abundant well-preserved bivalves, shell fragments and peloids (Figure 5 D2)		GS, EGS, and ZS	

241

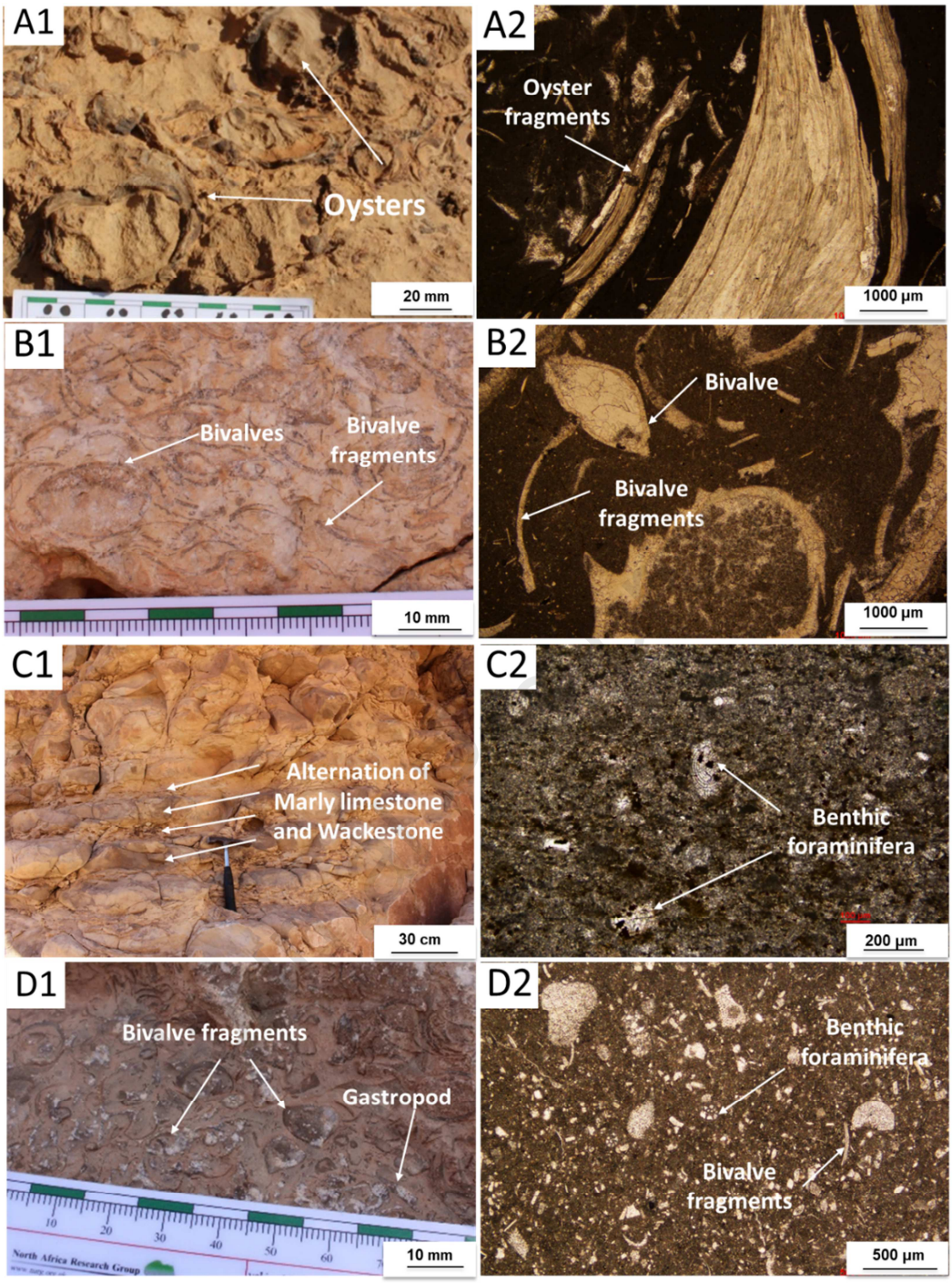

Figure 3. Illustration of LF 1 to LF4 lithofacies.

LF1: (A1) the Errachidia section, illustrating the oyster-rich dominated floatstone; (A2) Photomicrograph of the oyster-rich floatstone in the Errachidia section, LF2: (B1) the Errachidia section, illustrating the bivalve-rich floatstone; (B2) Photomicrograph, showing bivalves and bivalve fragments in the Tadighoust section. LF3: (C1) the Errachidia section, illustrating the thinly bedded wackestone alternating with marly limestone beds; (C2) Photomicrograph, displaying wackestone mainly composed of planktic and benthic foraminifera in the Tadighoust section. LF4: (D1) the Errachidia section, showing packstone with small bivalves, gastropods and some shell fragments; (D2) Photomicrograph of a packstone in the Errachidia section composed of shell fragments with foraminifera.

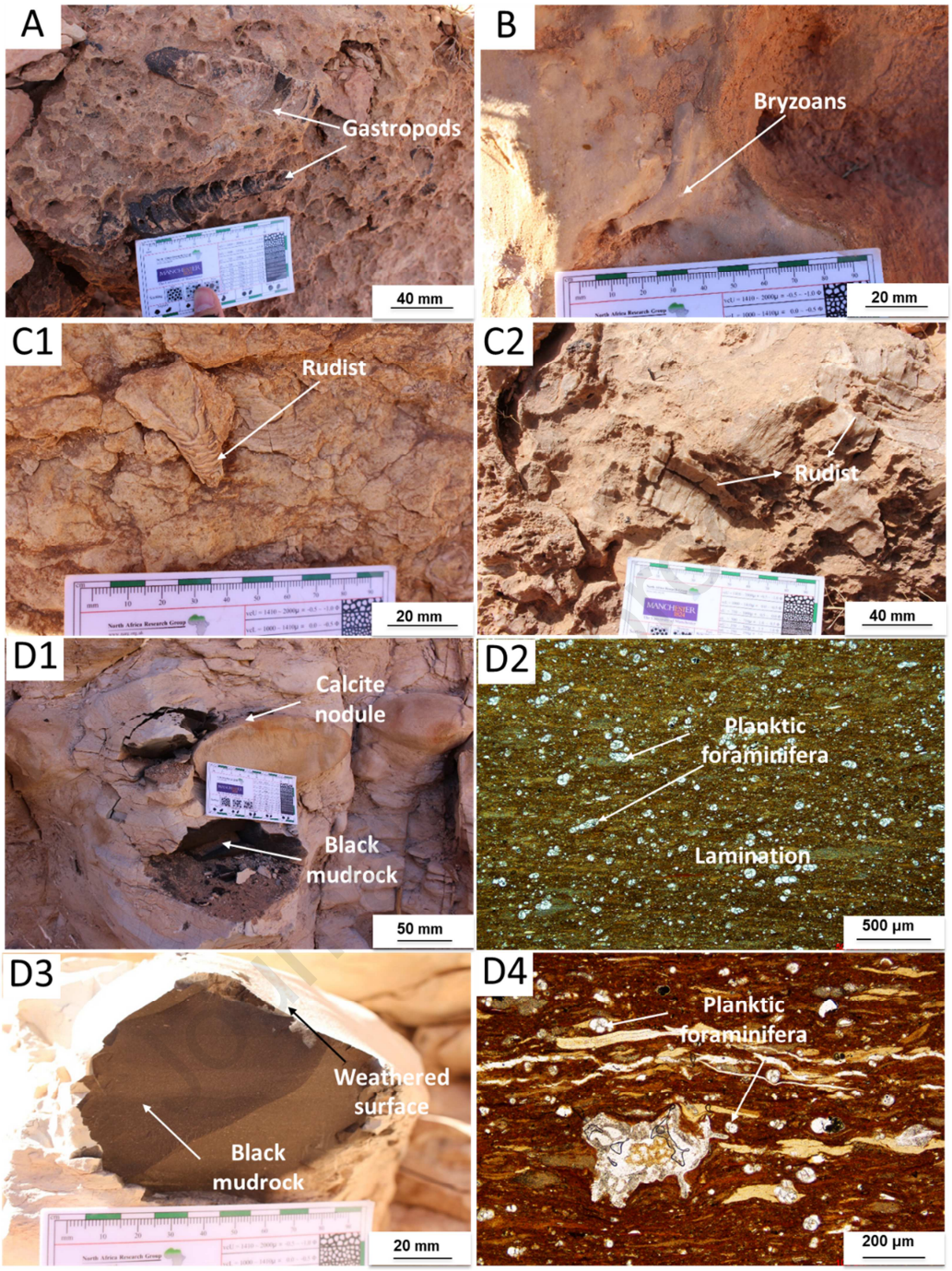

Figure 4. Illustration of LF4 to LF7 lithofacies.

LF5: (A) Zouala section, showing large weathered gastropod over 10cm; (B) Zouala section, showing the bryozoans in this lithofacies; (C1) Zouala section, rudist-rich floatstone, rudist shell still shows the well-preserved prismatic structures and some original microstructures though with some mud infilled; (C2) Ghaba Tarda section, view of slightly reworked rudists in LBL unit. LF8: (D1) the Errachidia section, showing highly weathered (weathering tan coloured) black mudstone and calcite nodules in black mudstone beds; (D2) Photomicrograph, showing lamination and abundant planktic foraminifera in the mudrocks; (D3) the Errachidia section, displaying fresh black and laminated mudrocks (D4) Photomicrograph, displaying crinoids and planktic foraminifera within the black mudstones.

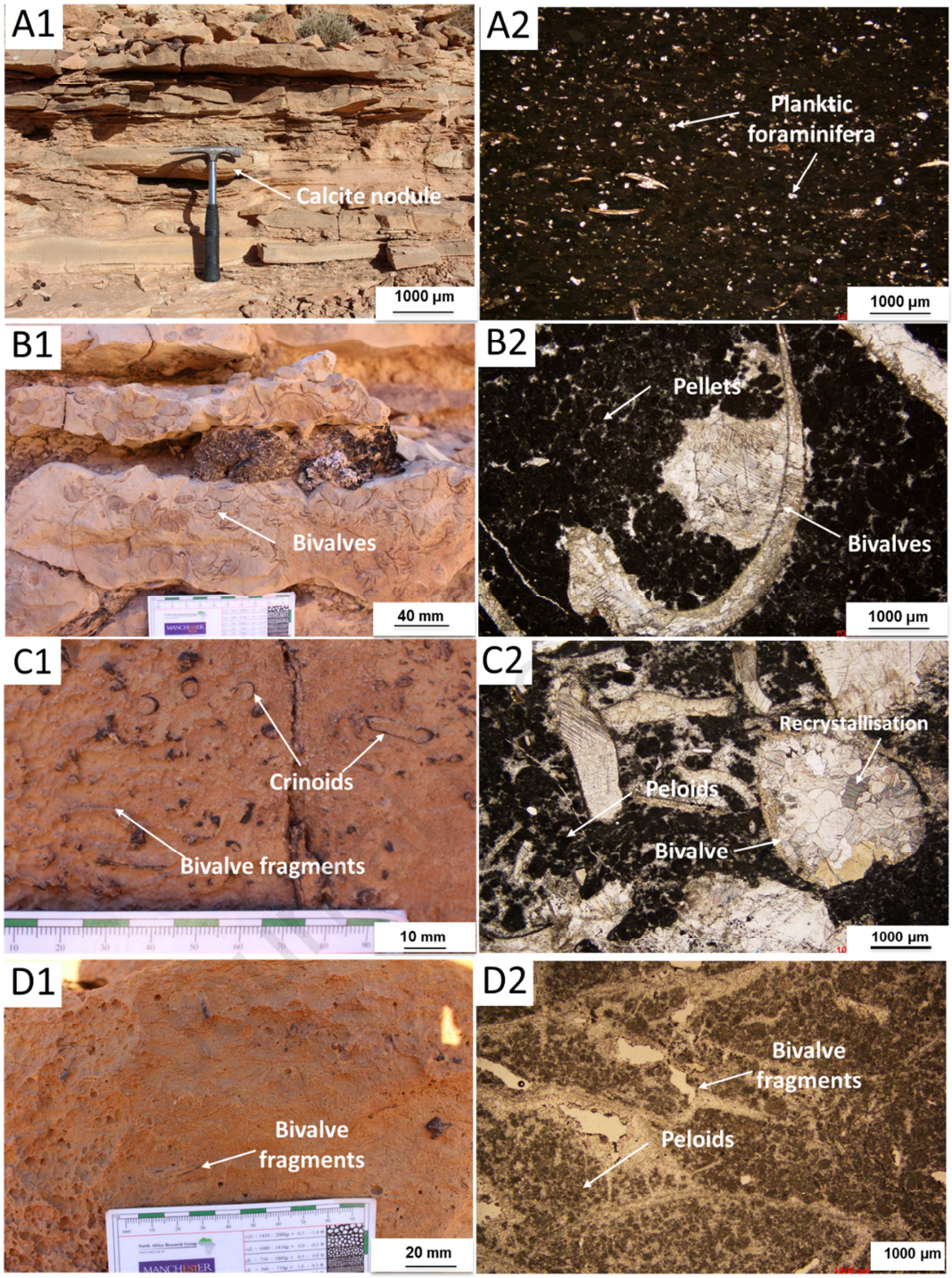

Figure 5. Illustration of LF9 to LF12 lithofacies.

LF9: (A1) the Goulmima section, illustrating nodular form of this lithofacies; (A2) Photomicrograph, presenting the planktic foraminifera and crinoid fragments. LF10: (B1) the Errachidia section, showing a nodular bivalve-rich floatstone interbedded with thin beds of marly limestone; (B2) Photomicrograph, bivalve-rich floatstone; LF11: (C1) the Errachidia section, illustrating the crinoids and bivalves rich floatstone; (C2) Optical micrograph, illustrating bivalves floatstone with abundant peloids in the Errachidia section; LF12: (D1) Goulmima section, showing the massive bivalves in this lithofacies; (D2) Optical micrograph, showing bivalves fragments with abundant peloids in the Goulmima section.

The dominance of fine-grained limestones (wackestone texture) and abundance of planktic foraminifera and crinoids in this unit suggest a low-energy environment in an outer-ramp setting, below the SWB. The vertical stacking pattern is interpreted to record a regional transgression that can be recognised across the whole area. However, the middle part of this unit is associated with LF10 and LF1, interpreted to record a change to a mid-ramp environment, suggesting a short interval of marine regression.

4.1.3. Upper Bioclastic Limestone (UBL) Unit

This unit comprises two main lithofacies and only accounts for a small part of studied sections (Figure 5). A thick package of floatstone-boundstone, mainly composed of bivalves, peloids and crinoids (LF11) is the dominant facies in the Errachidia, Errachidia West and Tadighoust sections, while in the Zouala, Ghaba Tarda and Goulmima sections this unit is dominated by LF12, containing abundant bivalves and peloids.

Both lithofacies are interpreted to represent deposition in a quiet subtidal water condition, suggesting a mid-ramp environment. This suggests a marine regression from the MFL unit.

Overall, based on the recorded lithofacies, the LBL unit is interpreted to record mid- to inner-ramp deposition, followed by dominantly outer ramp environment in MFL following a transgression. The UBL unit records a return to middle-ramp conditions.

Laterally, the southeast part of the studied area displays the shallowest environment of deposition based on the lithofacies associations, with deepening observed towards the north and west. The Errachidia section records the deepest water condition generally, with deposition of thick OM-rich black mudstone during the transgression of the MFL unit.

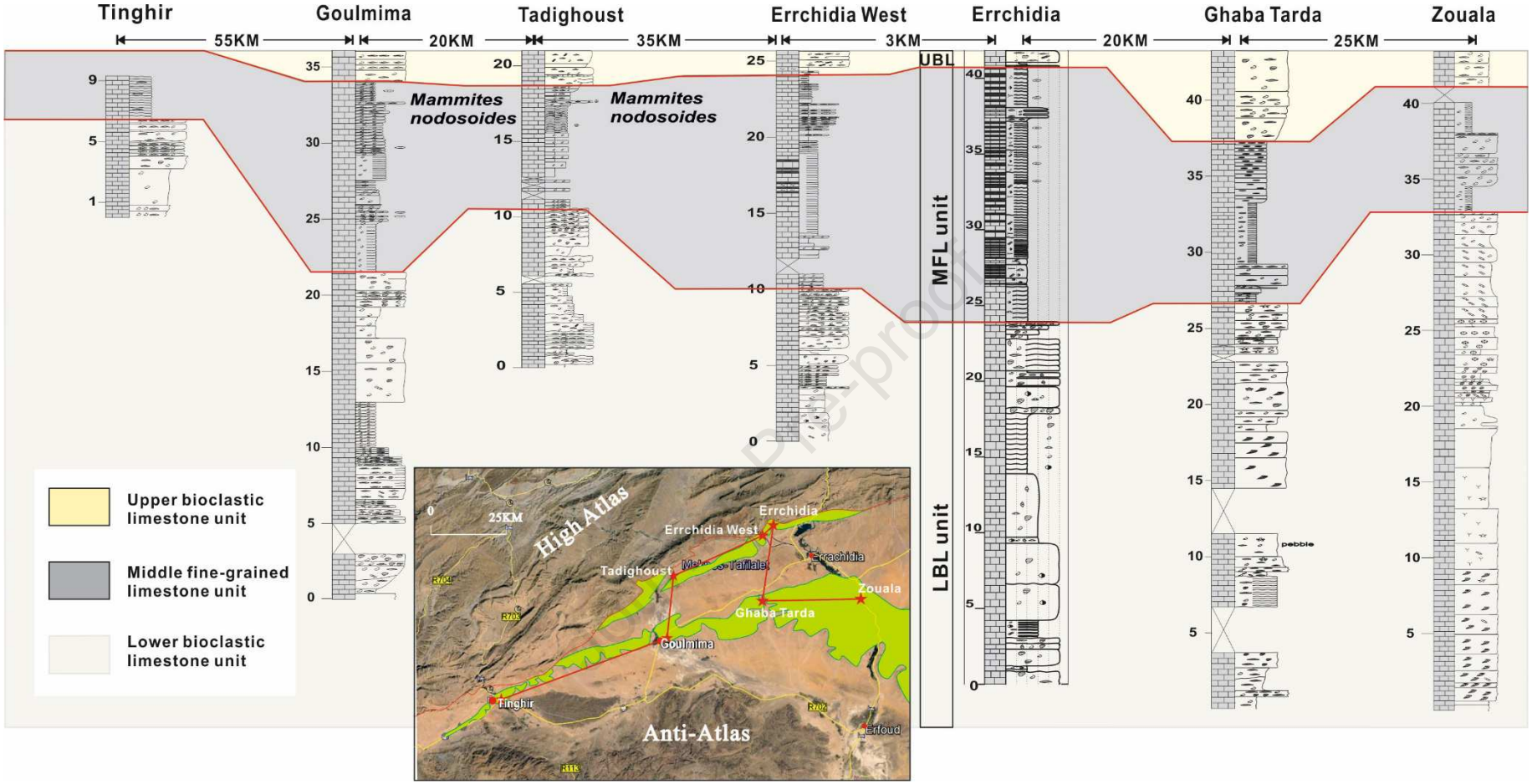

Figure 6. The lithological correlation of studied section of the Pre-African Basin. Three units were recognised: Lower bioclastic limestone unit (LBL), middle fine-grained limestone unit (MFL) and upper bioclastic limestoneunit(UBL).

4.2. **Distribution of organic-rich black mudstones**

In this study, OM-rich black mudstones were recognised in the Errachidia and Errachidia West sections. No previous study has reported this occurrence in the Pre-Africa Basin. Detailed sedimentological logging and both inorganic and organic geochemical analyses were undertaken on samples collected from the black mudstones and associated limestone strata, in order to evaluate their characteristics and assess the controls on organic matter accumulation and processes active in the carbonate platform environment.

The Errachidia section is located 15km north of Errachidia city, and the Errachidia West section is situated 3km west of the Errachidia section (Figure 1). The sections record similar lithological patterns, but much thicker organic-rich mudstone layers were recognised in the Errachidia section. Therefore, the Errachidia section (Figure 7) was chosen for the most detailed study of the Cenomanian-Turonian deposition in this area.

An association of LF1, LF2, LF3 and LF4 (Table 1) are recognised in the **LBL unit**, with LF1 and LF2 the two most common lithofacies, forming the lower and upper part of this unit. Three lithofacies (LF8, LF9 and LF10) (Table 1) are identified in the **MFL unit**, which has an overall thickness of 17m. This unit is significantly weathered at outcrop, hindering detail description. LF8 and LF9 are the best-developed lithofacies, forming bedding couplets, characterized as alternations of grey bioturbated limestone and black organic-rich mudstone.

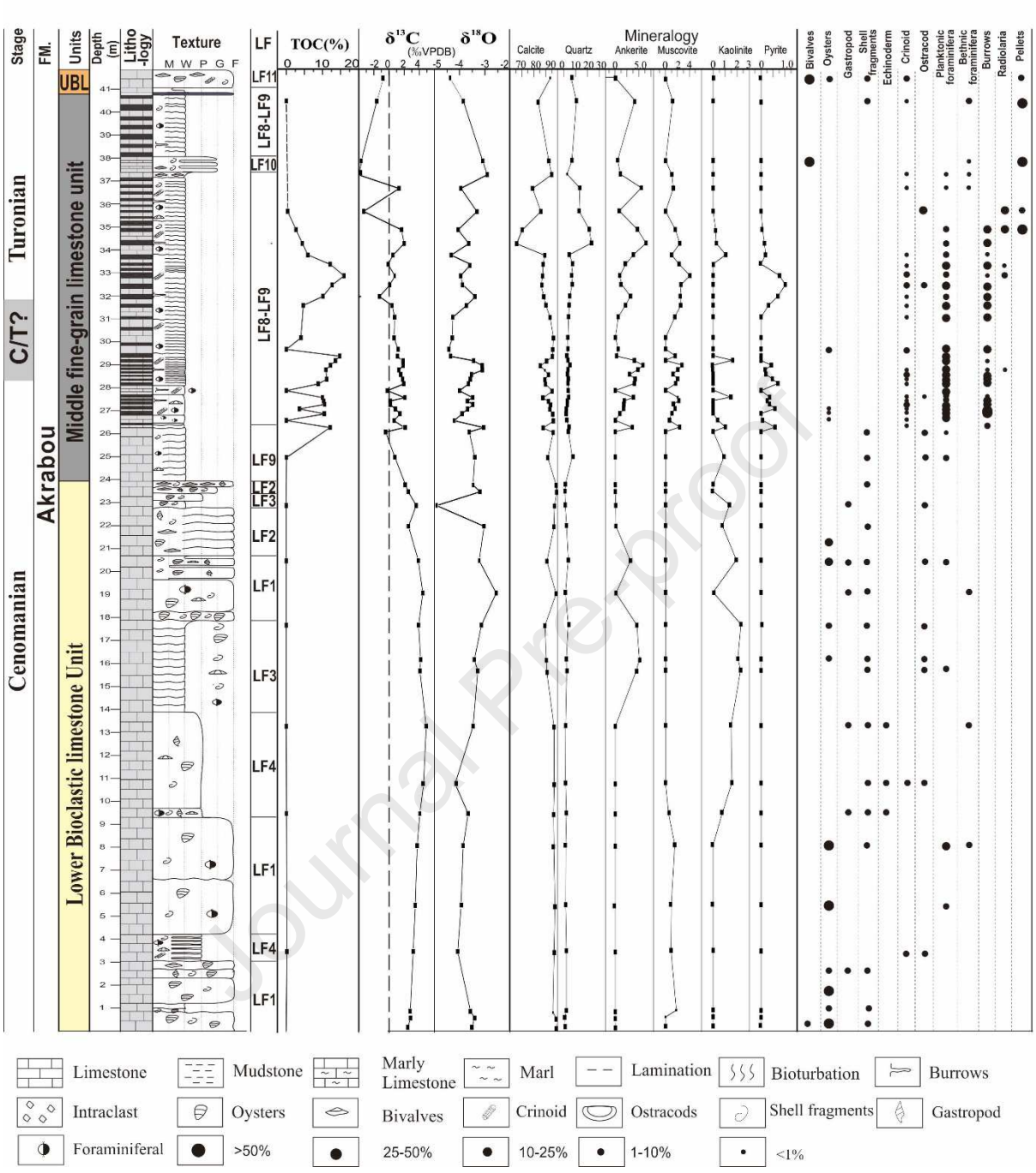

Figure 7. Cenomanian-Turonian succession of the Errachidia section showing the lithofacies, TOC values, fossils content and bulk rock mineralogy analysis

The black mudstones of LF8 contain abundant organic matter and have a bituminous smell when hit by a hammer. The TOC of the black mudstone (LF8) ranges from 2.7 wt% to 17.7 wt%, averaging 9.7 ± 3.9 wt% (standard deviation). It displays vertical variation throughout the unit (Figure 7). LF10 is only 1m thick, developed towards the

upper part of this unit. Most of the organic-rich mudstones have a high calcite content, ranging from 66% to 95% (average 90.1 ± 3%), with quartz values from 2.3% to 7.6 % (average 4.3 ± 1.5%) (Figure 7).

The overlying **UBL unit** is only 1m thick and comprises a package of bivalve and crinoid rich limestones (LF11) (Table 1).

4.3. **Biostratigraphy and chemostratigraphy**

A revised bio- and chronostratigraphic framework is proposed based on new material and analytical results obtained in the course of our study (including new identification of ammonites, planktic foraminifera and carbon isotope data) and a subsequent reinterpretation of published data (Figure 8).

4.3.1. Biostratigraphy

4.3.1.1. **Ammonites**

The nomenclature of the ammonite zones follows the definitions of the Southern Tethys and Western Interior Seaway zonation schemes (Meister and Piuz, 2013). Ammonoid species were mainly identified for specimens recovered from the Tadighoust section (previously called the Asfla section in Kennedy et al., 2008). Detailed logs published by Kennedy et al. (2008) and Meister et al. (2017) clearly show that the distribution of Turonian ammonites is not as restricted to the lower part of Unit T2 as suggested in previous literature, but can be found throughout the upper part of the lower Turonian. This is also supported by our own findings. Ammonoids occur, but are rare, within the nodule beds in the lower part of Unit T2, and become more abundant in the upper part of that interval (Figure 8).

352 *Vascoceras durandi*, *Hoplitoides* gr.*wohltmanni* and *Neoptychites cephalotus* co-occur in the
353 lowest ammonite horizon, while *Hoplitoides mirabilis* and *Fagesiaperoni* are recognised at a
354 slightly higher level in the Tadighoust section (Figure 8). The typical Lower Turonian *M.*
355 *nodosoides* Zone fauna was collected from upper part of Unit T2, and forms the highest
356 ammonite level. It include the index species, *Mammites nodosoides*, but also
357 *Nannovascoceras intermedium* that characterises the *M. nodosoides* Zone in Venezuela
358 (Kennedy et al., 2008; Meister et al., 2017).

359 4.3.1.2. **Planktic foraminifera**

360 Planktic foraminifera events provide a useful alternative biostratigraphic tool to characterize
361 the C/T interval. The biostratigraphic value of the most significant events that characterise
362 the *Rotalipora cushmani*, *Whiteinella archaeocretacea* and *Helvetoglobotruncana helvetica*
363 zones, was recently discussed at length by Falzoni et al. (2018). However, the discrepancies
364 and uncertainties of foraminiferal bioevents limited the biostratigraphic value in the Pre-
365 African Basin. In this study, *Planoheterohelix moremani* and *Whiteinella spp*.
366 (e.g.,*Whitenella archaeocretacea* and *Whiteinellabaltica*) are the dominant species in this
367 C/T succession. The"*Heterohelix*" shift event (Leckie, 1985; Leckie et al., 1998; Elderbak
368 and Leckie, 2016), which has been considered as a useful indicator that allows regional
369 correlation, is recognised in all the studied sections. The onset of "*Heterohelix*" shift (**HSO)**
370 has been recognised in the Erracchidia, Goulmima and Tadihoust sections based on the thin
371 sections analysis (Figure 7 and Figure 8). It is located in the lower part of the MFL unit
372 (Figure 8), which is consistent with the studies by Lezin et al. (2012).

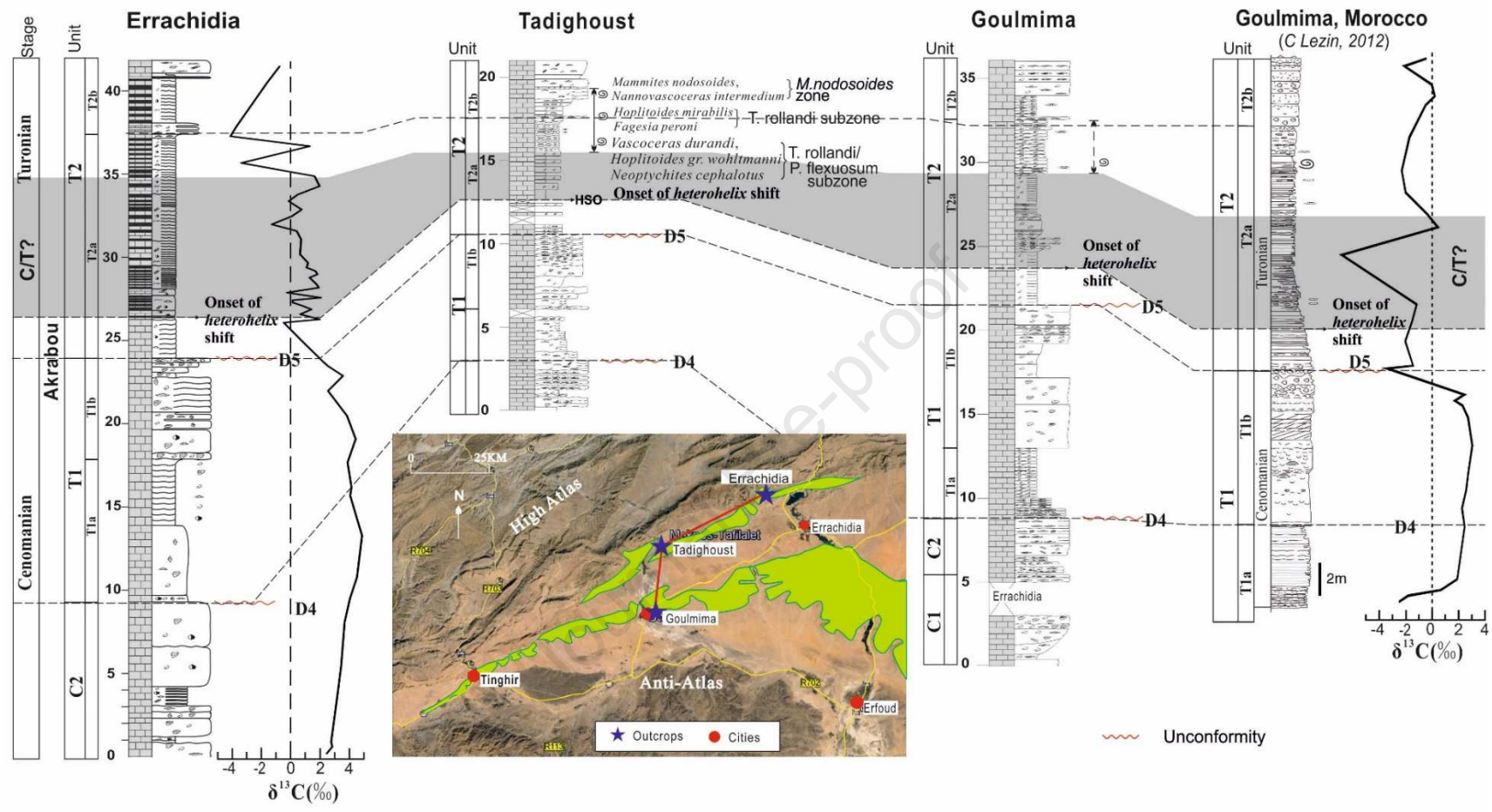

373

374 **Figure 8. Correlation of three studied sections in the Pre-African Trough. The subdivided units were identified based on Ettachfini and**
375 **Andreu (2004), and the carbon isotope data of Goulmima section was from Lézin et al. (2012)**

376

4.3.2. Carbon and Oxygen isotope stratigraphy

Carbon isotope and oxygen isotope analysis were conducted on samples from the Errachidia section (Figure 7) and compared to data published from other sections in this area reported by Lézin, et al. (2012) (Figure 10). The integrated results offer a better understanding of the palaeoenvironmental changes during the C/T interval in studied basin and establish a more robust C/T stratigraphic framework.

Bulk carbon isotopic analysis of 52 samples from the Errachidia section displays a wide range of $\delta^{13}C$ values from -4.09‰ to +4.90‰ (Figure 7). It should be noted that the carbon isotope values measured from the LBL unit and the lower part of MFL unit can generally be characterized as uniform (Figure 7). The $\delta^{13}C$ and $\delta^{18}O$ values of the bulk carbon plot within three clearly distinct fields (Figure 9). One data set (n=18), all from the LBL unit, has $\delta^{13}C$ values from +2.18 to +4.90‰ (mean 3.52‰, standard deviation = 0.76) and $\delta^{18}O$ values from -4.91 to -2.56‰ (mean -3.55‰, standard deviation = 0.49‰). The second data grouping (n=31), including samples from the MBL and UBL units, and displays $\delta^{13}C$ values from -+1.62 to +2.08‰ (mean +0.78‰, standard deviation = 1.60) and $\delta^{18}O$ values from -2.91 to -4.43‰ (mean -3.78‰, standard deviation = 0.72). The final grouping, all from the MBL unit, has the lowest $\delta^{13}C$ values (n=3), highlighted in Figure 9, with values from -3.35 to -4.09‰ (mean -3.71‰, standard deviation = 0.30) and $\delta^{18}O$ values from -3.05 to -3.11‰ (mean -3.08‰, standard deviation = 0.03) (Figure 9).

396

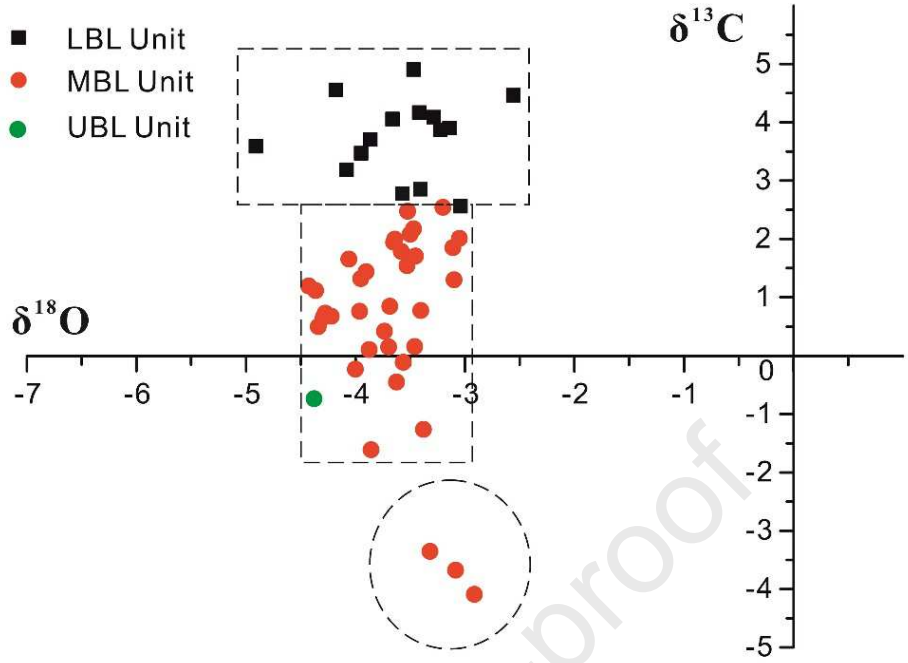

397

398 **Figure 9. $\delta^{13}C$ and $\delta^{18}O$ plot of C/T sediments in the Errachidia section.**

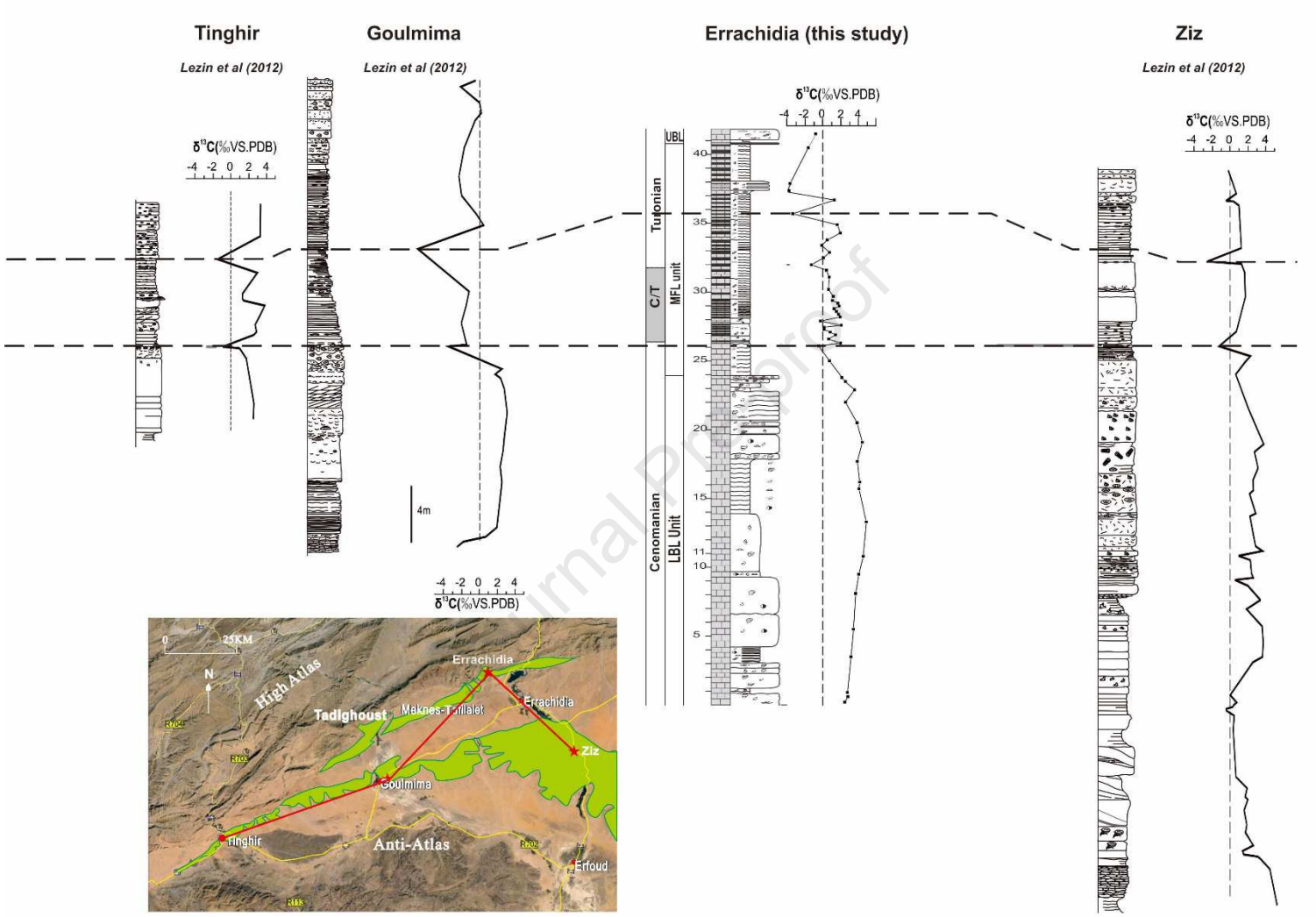

Figure 10. Cenomanian-Turonian succession of the Errachidia section with carbon and oxygen isotope curves, and correlation with carbon isotope curves of other sections by Lézin et al. (2012).

4.4 **Trace and Major Elements**

A suite of trace and major elements have been analysed on samples from the Errachidia, Tadighoust and Goulmima sections (Figure 11), to explore the geochemical response to spatial and temporal changes in palaeoenvironments associated with the different lithofacies.

Aluminium (Al), titanium (Ti), thallium (Th), and zirconium (Zr) are commonly utilized as proxies for terrigenous input (Tribovillard et al., 2006), and are generally associated with the terrigenous aluminosilicate fraction, clay minerals and some biogenic components. These detrital sensitive elements occur in relatively low concentration throughout the Errachidia section (Figure 11). The values are extremely low in both the LBL and UBL units, showing a depleted concentration, while slightly increased values are recorded in the MFL unit, which has a moderate concentration. The Tadighoust and Goulmima sections show similar trends to the Errachidia section (Figure 11), but with less concentration, indicating minor detrital influx. Overall, these detrital influx indicators displayed consistently low values in all the C/T sediments analysed in the studied area (Figure 11).

Phosphorus (P), nickel (Ni), zinc (Zn), and copper are commonly used palaeoproductivity indicators. Cu and Ni influx has been associated with marine organic matter in sediments (Tribovillard et al., 2006) and during organic matter preservation, these elements are generally more sensitive than P and Zn. Al-normalized elemental ratios are used to correct possible dilution by organic matter and authigenic minerals (Calvert and Pedersen, 1993; Morford and Emerson, 1999) (Figure 11). Elemental enrichment is based on comparison between the ratios of *Elements/Al* to a standard shale (Turekian and Wedepohl, 1961; Wedepohl, 1971; Calvert and Pedersen, 1993; Wedepohl, 1995; Morford and Emerson, 1999; Van der Weijden, 2002). These results display values of productivity-sensitive elements in both the LBL and MFL units that suggests a moderate to significant enrichment (Figure 11).

Higher average values are recorded in the MFL unit across the basin, showing high/extremely high enrichment. Maximum values are recognised in the middle part of this unit. The OM-rich mudstone interval in the MFL unit of the Errachidia section shows the highest concentration of these elements, interpreted to indicate significantly enhanced productivity associated with organic matter accumulation.

Co, Zn, Ni, U, Cr and V have also been considered as possible indicators of oxygen-depleted water conditions (Calvert and Pedersen, 1993; Brumsack, 2006; Fleurance et al., 2013), as they also show an association of generally higher concentrations in organic-rich sediments. However, some of these trace elements, such as Zn, Ba, Co and Cr, are readily remobilised after deposition, thus V, Mo and U are considered to be better redox-sensitive indicators (Tribovillard et al., 2006; Algeo and Tribovillard, 2009; Tribovillard et al., 2012). These elements are commonly applied and analysed together allowing the discrimination of dysoxic conditions from anoxic water conditions (Tribovillard et al., 2006).

In studied sections, the redox-sensitive elements V, Mo, and U show depleted to moderate concentration in both the LBL and UBL units. Samples throughout the MFL unit in the Errachidia section are associated with the highest concentration of all the elements, whilst in the Tadighoust and Goulmima sections, high values of enrichment were limited to certain elements in selected intervals.

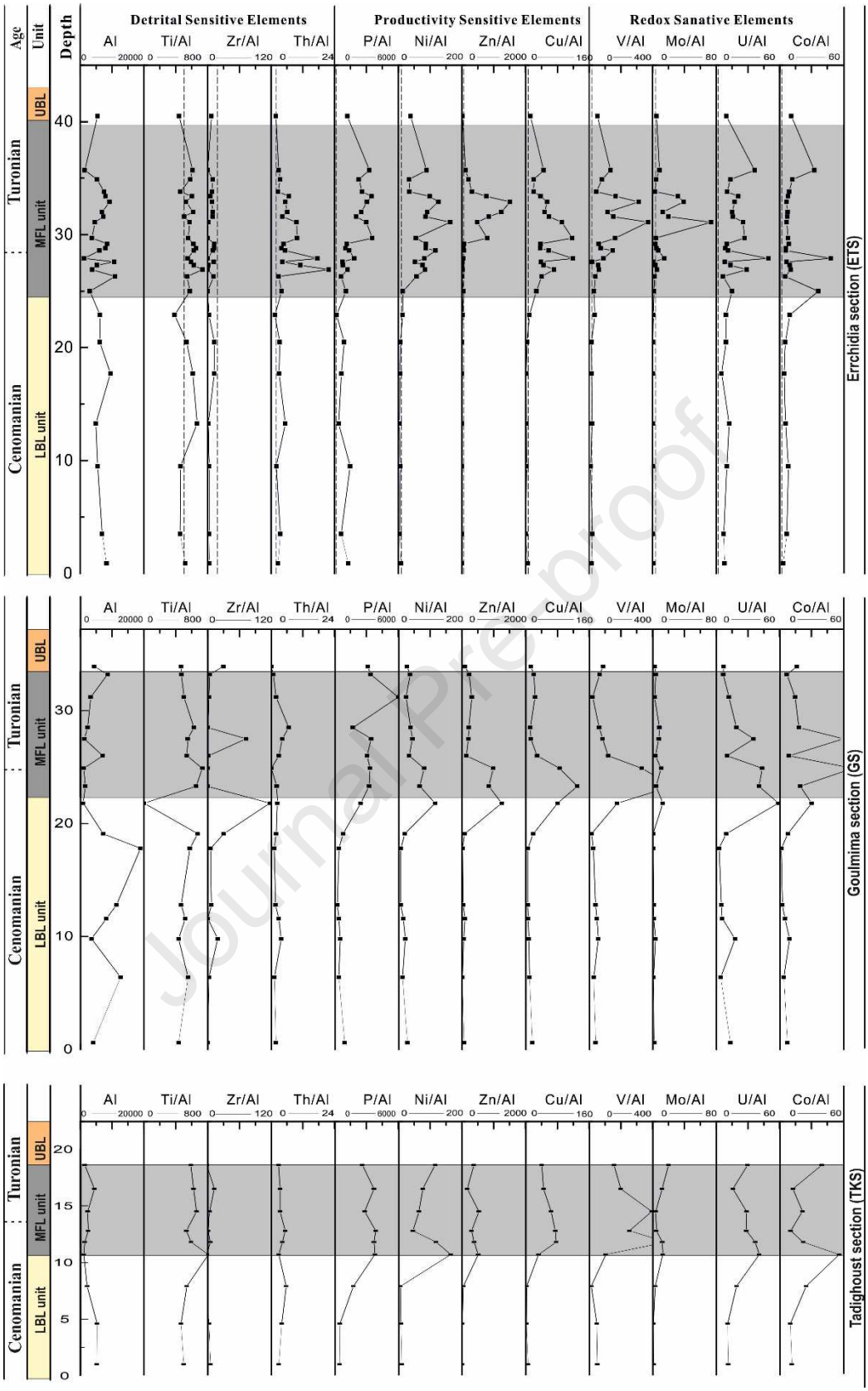

Figure 11. Enrichment proxies representing clastic factors for influx, redox conditions and productivity in the Errachidia, Tadighoust, and Goulmima sections.

5 Discussion

5.1 C/T boundary and OAE2 interval

5.1.1. Biostratigraphy

Ammonites have long been known to occur in the studied area (Basse and Choubert, 1959), although, despite their reported identification, the precise distribution of the faunas was not documented. A limited number of specimens were previously reported from Unit C1 at Tazzouguert and Unit T2 at Goulmima and Tadighoust (Figure 8) (Meister and Rhalmi, 2002; Ettachfini and Andreu, 2004), but it was only in recent years that the larger faunas were formally described (Kennedy et al., 2008; Gale et al., 2017; Meister et al., 2017).

The co-occurrence of ammonite species *Vascoceras durandi*, *Hoplitoides* gr.*wohltmanni*, and *Neoptychites cephalotus* found in the Tadighoust section, are known to range through the *P. flexuosum* and *T. rollandi* subzones of the lowest Turonian *W. coloradoense* Zone (Meister and Piuz, 2013) but it does not allow discrimination between the two subzones (Figure 8). The in-situ specimen of *Vascocerascompressum* reported by Meister et al. (2017), is a junior subjective synonym of *Vascocerasproprium*, and supports that the *P.flexuosum* subzone is represented at the Tadighoust section (Kennedy et al., 1987; Courville, 1993) . The recognition of *Hoplitoides mirabilis* and *Fagesiaperoni*in the middle part of the Tadighoust section leaves no doubt that this level belongs to the upper part of *T. rollandi* subzone. The highest ammonite species, *Mammites nodosoides* and *Nannovascoceras intermedium*, are typical species from the lower Turonian *M. nodosoides* Zone. The fauna found also include *Romaniceras (Yubariceras) reymenti*, which is a common element of the *M. nodosoides* Zone of the Tarfaya Basin (LGB pers. observation). As discussed above, the successive ammonite faunas found in Unit T2 indicate the *W. coloradoense* (*P. flexuosum* and *T. rollandi*

subzones) and *M. nodosoides* zones of the Lower Turonian (Figure 8). This re-interpretation together with new faunal identification suggests that the proposition by Lézin et al. (2012), that this section only shows the occurrence of the fauna associated with the *M. nodosoides* Zone can definitively be ruled out. None of the ammonites documented so far allow the recognition of the basal Turonian (*W. devonense* Subzone of the *W. coloradoense* Zone). Therefore, the precise position of the C/T boundary cannot be identified by means of ammonite biostratigraphy alone.

Planktic foraminifera bioevents commonly serve as a complementary tool to improve precision in C/T stratigraphy studies. The interpretation of Lebedel et al. (2015), who stated that three planktic foraminifera zones were recognised in the Akrabou Formation based on the discontinuous distribution of foraminifera identified from samples recovered from the Tazzouguert and Goulmima sections (Lézin et al., 2012), should be tempered. According to Lézin et al. (2012), the transition between the *Rotalipora cushmani* and *Whiteinella archaeocretacea*zones lies in the lower part of the Akrabou Formation (Unit C1, Ettachfini and Andreu, 2004). In our opinion, the recognised planktic formainifera species are insufficient to identify the biozone boundaries in this study, but the commonly identified onset of the "*Heterohelix* shift" (HSO) below the first occurrence of the Lower Turonian ammonites in the studied sections, is useful to characterise the C/T interval (Figure 8). The **HSO** was first identified in the Western Interior Seaway (Leckie, 1985; Leckie et al., 1998), as an abrupt change in planktic foraminiferal assemblages (see discussion *in* Elderbak and Leckie, 2016; and Falzoni et al., 2018). The biserial species *Planoheterohelixmoremani* and *P. globulosa* dominate the assemblage, and this change has been interpreted as an ecologic event resulting from a period of unstable eutrophic surface water conditions that inhibited the proliferation of the keeled K-strategist taxa. It should be noted that the **HSO** shift is likely diachronous across low to mid-latitude localities, but despite this, it always occurs in the

latest Cenomanian (Caron et al., 2006; Falzoni et al., 2018). In Morocco (i.e., High-Atlas, Middle-Atlas and High Moulouya), the highest occurrence (**HO**) of *Hedbergella* (*Asterohedbergella*) *asterospinosa* had been taken (Ettachfini et al., 2005; Sandoval et al., 2008) to mark the base of the C/T boundary. However, as this species does not appear in the syntheses of planktic foraminifera mentioned above, its biostratigraphic value is difficult to evaluate.

Therefore, neither ammonites nor planktic foraminifera allow the precise recognition of the position of the C/T boundary. The above results and dicussions suggest the interval of uncertain age control containing the C/T boundary ranges from the **HSO** to the lowest occurrence of Turonian ammonites. It merely corresponds to a time equivalent that includes the uppermost Cenomanian *N. juddii* Zone and the lowermost Turonian *W. devonense* Zone. Compared to our predecessors, we place the C/T boundary at a higher level in the Akrabou Formation (shown as the 'grey shadow' interval on Figure 8). As a consequence, in our interpretation, unconformities D4 and D5 fall within the Late Cenomanian and none of them mark the C/T boundary. This new biostratigraphic framework has significant implications for the interpretation and calibration of the $\delta^{13}C$ curve by comparison with reference sections at Wadi Bahloul and Pueblo.

5.1.2. Carbon Isotope Stratigraphy

The carbon isotope curve, as a chemostratigraphic proxy, has been widely applied in C/T stratigraphic studies. Regional and global correlation to biostratigraphy demonstrates that carbon isotope curves can be a powerful additional tool for high resolution C/T stratigraphic studies (Jenkyns, 1980; Scholle and Arthur, 1980; Pratt and Threlkeld, 1984; Tsikos et al., 2004; Caron et al., 2006; Sageman et al., 2006; Lowery et al., 2014; Falzoni et al., 2018). Plots of $\delta^{13}C$ and $\delta^{18}O$ data from C/T sediments in the Errachidia

519 section show three clearly distinct clusters (Figure 9). This suggests there is some
520 relationship between isotopic values and lithofacies in the Errachidia section, with more
521 positive $\delta^{13}C$ values in skeletal-rich lithofacies (Figure 7). However, the various isotopic data
522 occur in the same lithofacies, and similar values are identified among different lithofacies.
523 This might suggest the lithofacies is not the dominant control on the isotopic values. The
524 $\delta^{13}C$ values in the area denoted by the two rectangles in Figure 8 show no significant
525 recrystallisation based on the petrographic analysis. The narrow range in the $\delta^{18}O$ values
526 throughout all samples, in contrast to the $\delta^{13}C$ values means that diagenetic alteration and re-
527 setting of the $\delta^{18}O$ values are highly possible and cannot be ruled out.
528 Moreover, comparable $\delta^{13}C$ shifts are also recognised in other sections of the studied basin
529 (Figure 10). The different $\delta^{13}C$ in the two rectangle areas are more-likely due to global
530 changes in oceanic $\delta^{13}C$ properties related to the Oceanic Anoxic Event. This supports the
531 correlation of the $\delta^{13}C$ shift with the global reference sections (Figure 12).

532 The three outliers, denoted by the circles in Figure 8, show low $\delta^{13}C$ values that probably do
533 indicate some early cement in these sediments, associated with bacterial processes, which
534 decomposed the organic carbon, resulting in more negative $\delta^{13}C$ values. Therefore, the data
535 for the sediments from these three points are likely to be altered by diagenesis and should be
536 ignored for stratigraphic purposes. Overall, the range of $\delta^{13}C$ values, except the three circled
537 clusters, show no or little diagenetic modification of the primary isotopic composition and
538 suggest they can be used for regional and global correlation.

539 The C/T successions of the Wadi Bahloul section (Tethys Ocean influenced deposits) in
540 Central Tunisia and the Pueblo sections in USA have been widely studied in terms of
541 biostratigraphy and carbon isotopic stratigraphy(Tsikos et al., 2004; Kolonic et al., 2005;
542 Caron et al., 2006; Sageman et al., 2006; Falzoni et al., 2018). These two sections have good

age control, with the C/T boundary and biostratigraphical zones well defined. Three distinct $\delta^{13}C$ peaks were identified in the $\delta^{13}C$ profile during the OAE2 interval in both sections (Kennedy et al., 2005; Caron et al., 2006; Falzoni et al., 2018). Peak I is generally present at the top of the *R. cushmani* Zone, while the Peak II and Peak III are located in the *W. archaeocretacea* Zone. Peak III (Peak C in some references) is considered to be close to the C/T boundary (Caron et al., 2006; Jarvis et al., 2011; Falzoni et al., 2018) (Figure 12). According to the correlation, the onset of the OAE2 interval is generally below the Peak I, and terminated in the *W. devonense* Zone, commonly before the 'Trough a' (Figure 12) (Tsikos et al., 2004; Kennedy et al., 2005; Kolonic et al., 2005; Kuhnt et al., 2005; Jarvis et al., 2011; Košťák et al., 2018).

The absence of *R. cushmani* Zone indicates that Peak I is not recognised in the studied Errachidia section (Figure 12). A combination of the biostratigraphic and carbon isotopic curve correlations suggests the C/T boundary should be below the 'Trough a' of the $\delta^{13}C$ profile, recorded in both the Wadi Bahloul and Pueblo section in *W.devonense* Zone (Figure 12). Moreover, as Peak III is commonly present before the C/T boundary, but after the onset of **HSO** (Falzoni et al., 2018) and we recognize Peak III in the lower part of the 'grey shadowed zone', this places the C/T boundary of the Errachidia section based on the correlation (Figure 12). Ammonite zones recognised in this section, integrated with the $\delta^{13}C$ curve correlation, allow us possibly to establish the age of the ammonite and planktic foraminifera zones in this area (Figure 12).

Given this observation and the $\delta^{13}C$ correlation (Figure 12), the OAE2 interval in the Errachidia section should start below the studied LBL unit and end before 'Trough A' with a negative value. This indicates the OAE2 interval in the studied area includes the LBL unit and lower MFL unit and that the C/T boundary in the Errachidia section is identified in the

lower part of the MFL unit. Therefore, the recorded organic-rich black mudstones developed from the latest Cenomanian to early Turonian, equivalent with upper OAE2 interval to post OAE2 interval.

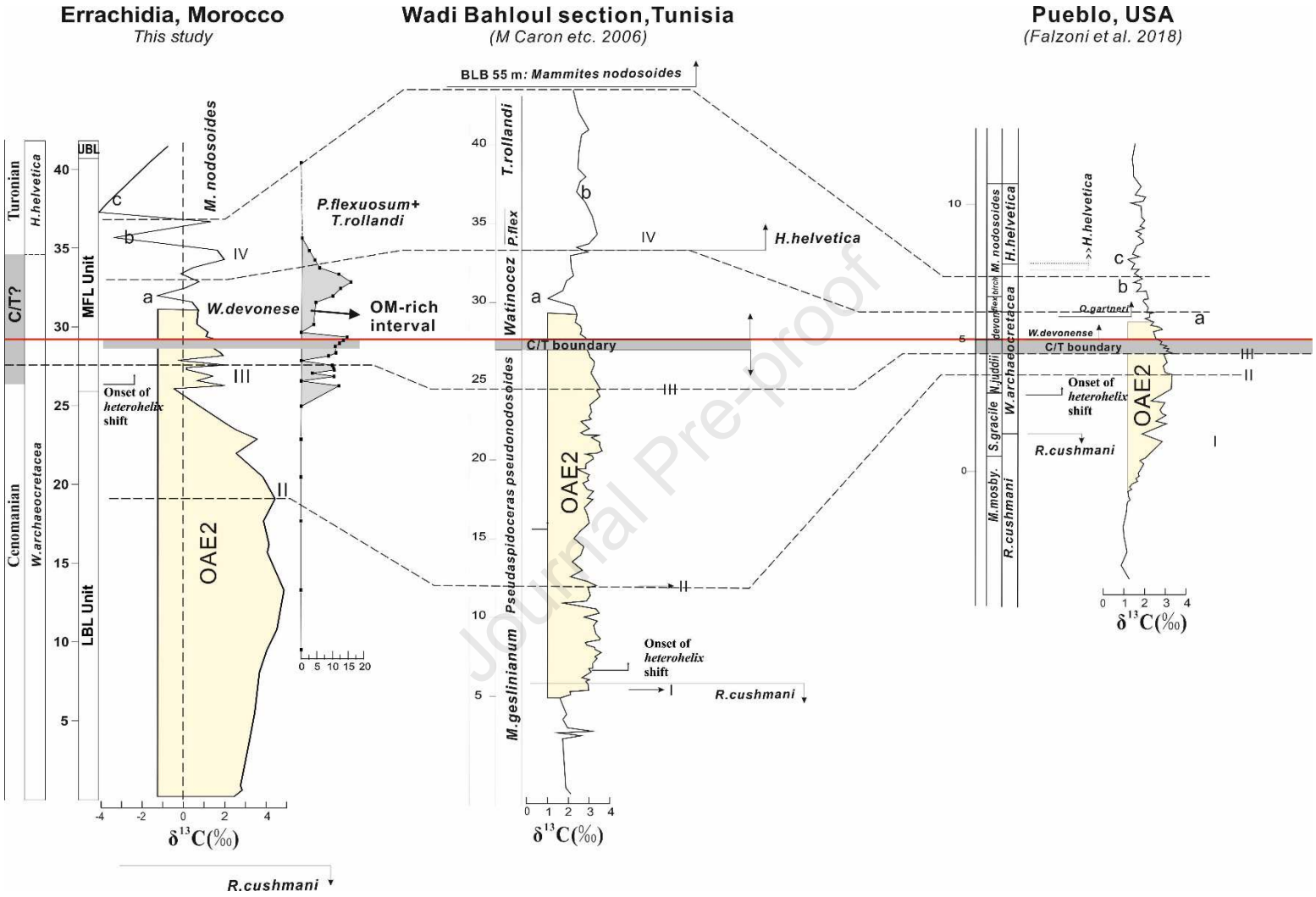

570

571 **Figure 12. Carbon isotope curve correlation with the Wadi Bahloul sections (Tethys ocean influenced), and the Pueblo section in USA**
572 **(GSSP for the base of the Turonian; Kennedy et al., 2005).**

5.2. **Palaeoenvironmental Implications**

5.2.1. Palaeoenvironments

Palaeoenvironments during the Cenomanian/Turonian interval in the Pre-African Basin are inferred from the lithofacies associations and redox-sensitive element analysis. Multiple other proxies, such as Ni/Co-U/Th and Mo-TOC have also been applied for the environmental analysis (Jones and Manning, 1994; Tribovillard et al., 2006; Tribovillard et al., 2012; Dickson et al., 2016).

As previously discussed, the LBL unit was deposited during the latest Cenomanian, corresponding to the OAE2 interval, typified by a positive $\delta^{13}C$ excursion. However, OM was below detection limits in these sections, which are commonly associated with bioclastic-rich limestone deposition, indicating a relatively shallow, well oxygenated marine environment. The extremely low concentrations of redox-sensitive trace element (V, Mo, and U) indicate that predominantly oxic water conditions prevailed during deposition of the LBL unit (Figure 13). Therefore, the typical OAE2 related anoxic conditions did not influence this part of the carbonate platform, and there is no evidence of anoxia at this time. Globally the OAE2 interval is commonly associated with high detrital influx and anoxic conditions (Du Vivier et al., 2014). The slight increase in detrital sensitive element concentration (Al, Ti, Zr, and Th) and the local recognition in the LBL unit of dysoxic bottom water conditions (in the Goulmima section) (Figure 13), might be associated with influence of the OAE2 (Van Helmond et al., 2014), but the detrital-sensitive trace element (TE) enhancement is insignificant. This is likely a result of the shallow nature of our study area during the OAE2 interval, which is consistent with similar responses reported during the OAE2 in other shallow carbonate platform deposits (Elrick et al., 2009; Korbar et al., 2012).

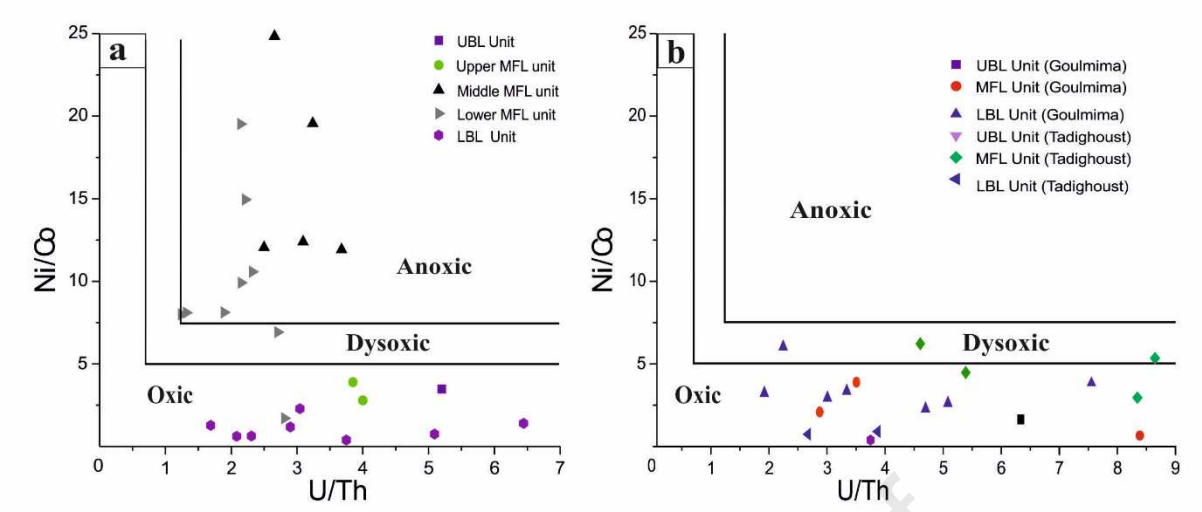

596

597 **Figure 13. The cross plot of trace element ratios as palaeoredox proxies in the Errachidia (a)**
598 **and Goulmima and Tadighoust sections (b), based on Jones and Manning (1994) and Hatch and**
599 **Leventhal (1992).**

600 However, the presence of LF8/LF9 in the lower MFL unit of the Errachidia section and LF9
601 in the other sections, suggests a deepening occurred across the entire area. This interval
602 shows evidence for more variable redox water conditions. In the Errachidia section, the
603 significant enrichment of most redox-sensitive trace elements (Figure 11) suggests deposition
604 of organic-rich mudstones under anoxic water conditions (Figure 13), whilst the inter-bedded
605 greyish organic-poor mudstones were deposited in dysoxic/oxic water conditions. The redox-
606 sensitive TE concentrations also show an increase at the equivalent level in the Goulmima
607 and Tadighoust sections. However, these elements remain depleted or only show moderate
608 enrichment (Figure 11), suggesting prevailing oxic water, with sporadic dysoxic conditions
609 (Figure 13). The documented anoxic conditions in the Errachidia section and oxic/dysoxic
610 conditions in the other sections, suggest that although a regional marine transgression
611 occurred in the whole area, anoxia was only developed at the deepest site.

612 At the base of Lower Turonian, strata possess a decreased OM content in the Errachidia
613 section and an increased bioclastic component in the nearby sections, suggesting a fall in sea
614 level and regional shallowing. This is overlain by deeper marine sediments across the whole

615 basin, indicated by a change to dominantly fine-grain sediments and the significant increase
616 in redox-sensitive element concentration (Figure 11). This is most marked in the Errachidia
617 area, which records the maximum TE and organic matter concentration. The subsequent
618 increase in bioclastic content and decrease in redox-sensitive element concentration in the
619 upper MFL unit records another relative sea-level fall. This is also supported by the
620 substantially decreased organic matter content in the Errachdia section and increased
621 bioclastic content in the other sections.

622 Bioclastic-rich limestone deposition dominates the UBL unit across the whole basin,
623 suggesting well-oxygenated bottom water conditions. This is supported by the low trace
624 elements concentration. This suggests shallow marine deposition and increased oxygen
625 content in the water column owing to a rapid marine regression in the upper Lower Turonian.

626 Overall, oxygen depleted water conditions occur in all the studied areas from the latest
627 Cenomanian to early Turonian, which when correlated to the carbon isotope curve, is coeval
628 to the latest OAE2 and post-OAE2 stage (Figure 14). Anoxic/euxinic water conditions were
629 only recognised in the Errachidia section suggesting oxic water condition prevailed across the
630 basin during the lower OAE2 interval, which was not favourable to organic carbon
631 preservation. In contrast to many published reports that examine the OAE2 interval in deep
632 water open marine environments (Jarvis et al., 2011; Kuhnt et al., 2017), in the shallow water
633 platform and intra basinal areas of the Pre African Basin, the onset of anoxic-euxinic water
634 conditions only began from the Peak III of $\delta^{13}C$ curves. Oxygen-depleted water conditions
635 did not appear until the latest Cenomanian and were maintained only until the early Turonian,
636 intercalated periodically with oxic/dysoxic conditions. It is clear that the majority of the fine-
637 grained limestone and associated OM-rich deposits related to dysoxic-anoxic-euxinic water
638 conditions were deposited after the OAE2 interval (Figure 14). This has also been recognised

639 in the Gulf of Mexico shelf (Lowery et al., 2017) and the Mexican carbonate platforms
640 (Hernández-Romano et al., 1997; Elrick et al., 2009; Omana et al., 2012; Núñez-Useche et
641 al., 2016) during the C/T interval.

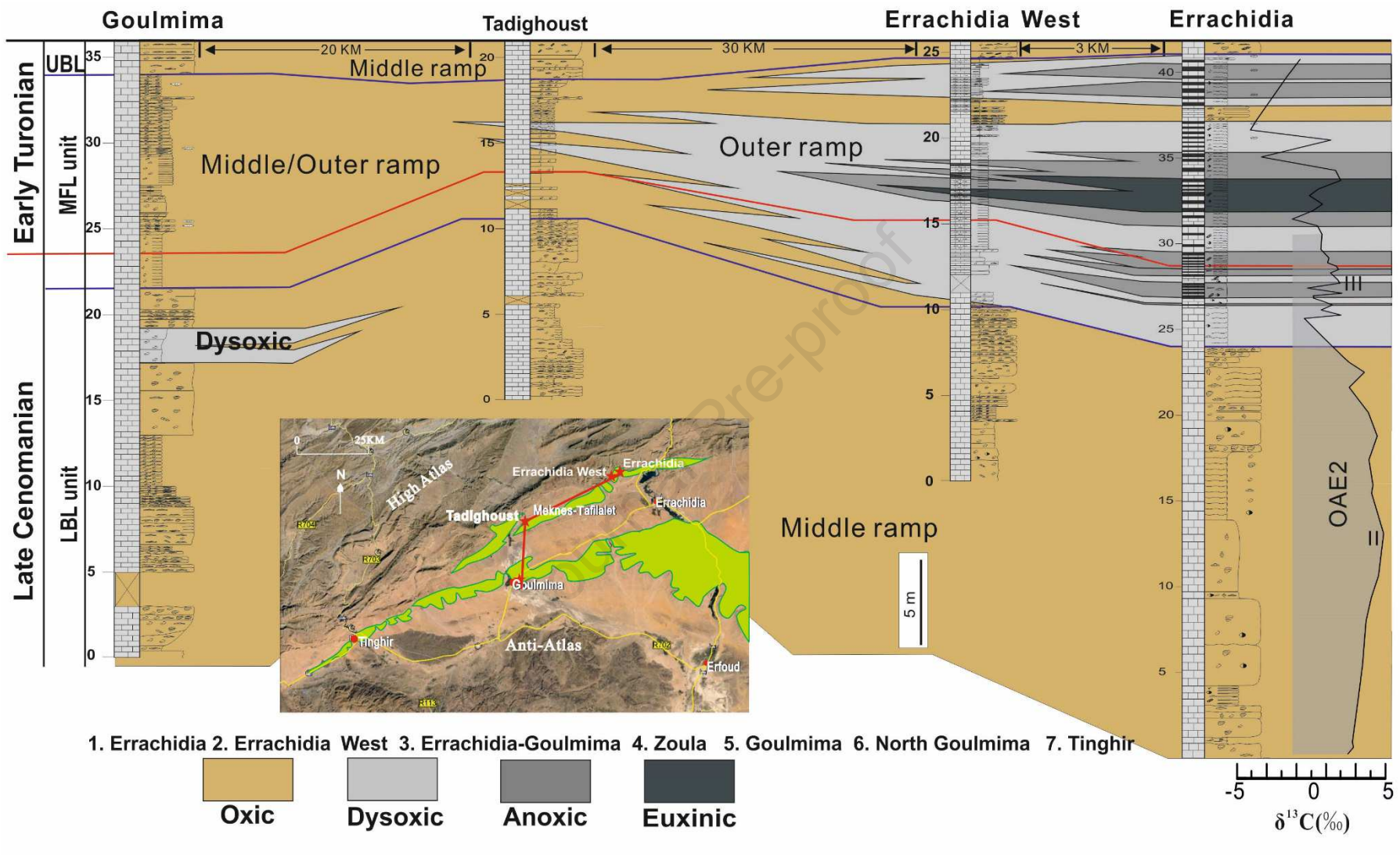

Figure 14. Stratigraphic correlation and depositional environments in the Errachidia and its adjacent sections.

5.2.2. Relative Eustatic Sea level

Correlation of eustatic cycles with the sediment record, based on ammonite zones and carbon isotope profiles, shows an association of the organic-rich mudstones interval (MFL unit) in the Errachidia area with the late Cenomanian and early Turonian marine transgressions (Figure 15). However, OM-rich mudstone deposition in this basin is located in the upper OAE2 interval, suggesting a delayed response compared to the global late Cenomanian transgression, which is typically coeval with the onset of OAE2 interval (Keller et al., 2004; Haq, 2014) (Figure 15). This suggests that local depositional controls and topography influenced relative sea-level played an important role.

A regional correlation with other Tethyan C/T sections in Algeria (the Chebeibita section) (Figure 16) illustrates a comparable scenario to that recorded from the Pre-African Basin in Morocco, whereby organic carbon is locally distributed and started to accumulate from the upper OAE2 interval (Grosheny et al., 2008). However, in the more distal Oued Bahloul section of Tunisia (also Tethyan-influenced), organic matter enrichment is coeval with the onset of the OAE2 interval(Aguado et al., 2016). This suggests that the marine transgression that occurred in the Tethyan Moroccan basin is more likely an interplay of eustasy and local tectonics. In contrast, the OM-rich mudstones in the middle MFL is coeval with the early Turonian transgression, and OM-rich mudstones are also widely recognised in the other Tethys Ocean influenced basins (Figure 16), such as the more distant Oude Bahloul section in Tunisia (Aguado et al., 2016), and in the US Western Interior Seaway(Sageman et al., 2006; Elderbak and Leckie, 2016). A short interval of marine regression associated with the increased bioclastic deposition and decreased OM matter is recorded in the basal part of the post-OAE2 interval in this study. These sea level changes are strongly consistent with the global short-term sea level curves (Sloss, 1963; Sageman and Bina, 1997; Friedrich et al.,

668 2012; Haq, 2014; Jarvis et al., 2015). These suggest the maximum early Turonian sea level
669 rise probably represents a global signal, which exerted the dominant control on organic-rich
670 mudstone deposition.

671 To conclude, the organic-rich mudstones in this Tethyan Moroccan basin show influence by
672 global marine transgression, with drowning of the continent and development of relative
673 deeper palaeoenvironments the main control on OM-rich mudstone deposition.

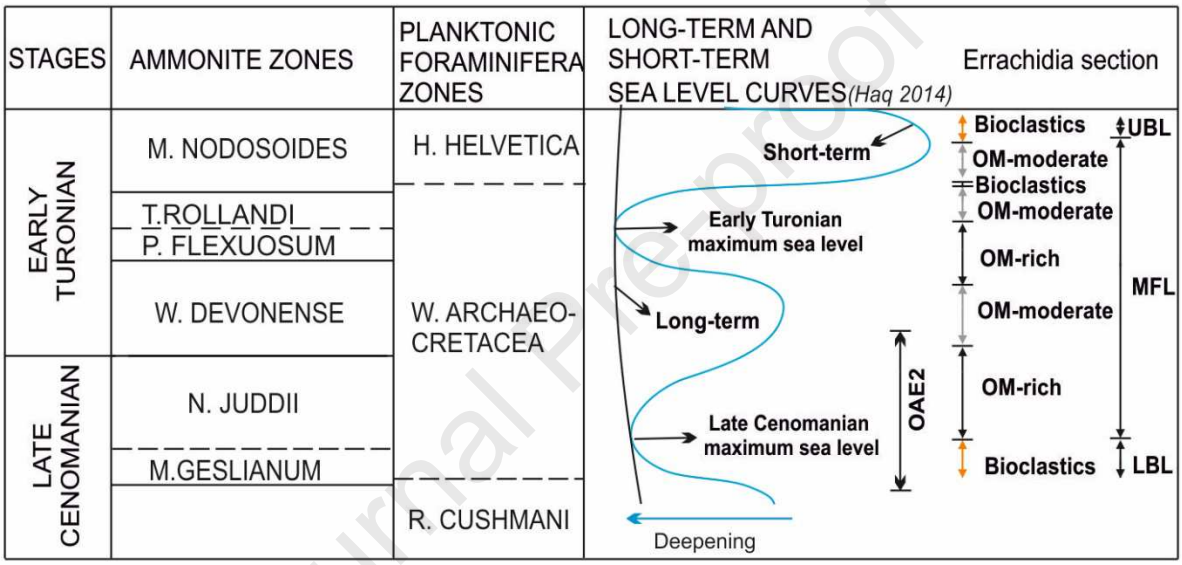

674

675 **Figure 15. The correlation between global sea level curves and sediments in the Errachidia**
676 **section based on biostratigraphy.**

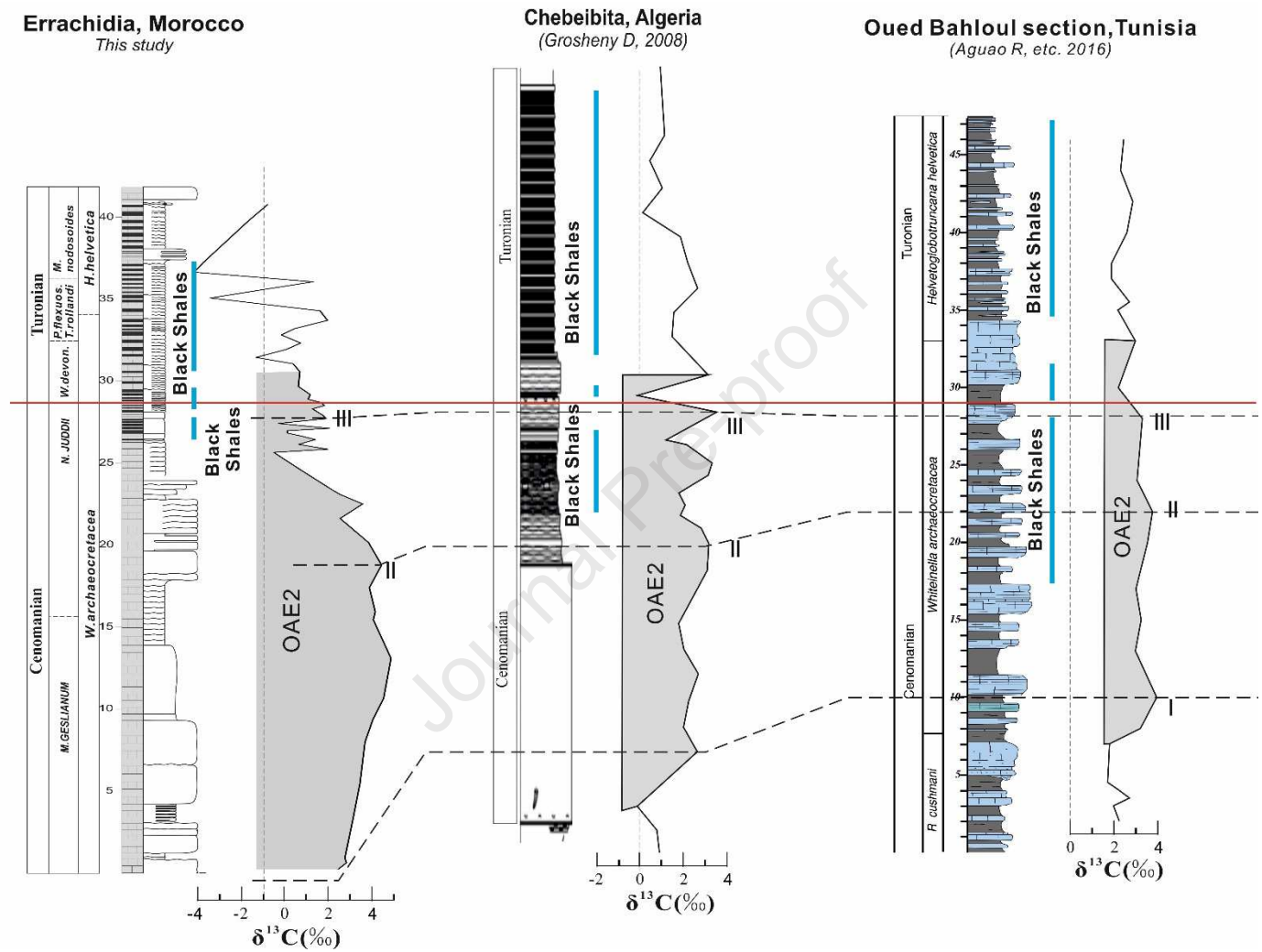

677

678 **Figure 16. Correlation of carbon isotope curves between Tethys ocean influenced basins across North Africa.**

5.3. **Controlling factors of OM-rich black mudstone deposition**

The palaeoenvironment and sea level interpretation suggests shallow marine conditions prevailed over the whole basin before the regional late Cenomanian marine transgression. The Errachidia section shows a comparable lithofacies assemblage with the nearby Goulmima and Tadirhoust sections during the LBL unit (Table 1).

Although the whole basin records a response to the late Cenomanian/early Turonian marine transgressions, high concentrations of organic matter are only recognised in the Errachidia area, where more reducing bottom waters existed. The record of organic-rich mudstones are rare on shallow carbonate platforms globally across the OAE2 interval (Elrick et al., 2009; Korbar et al., 2012), ascribed by most authors to the dominance of oxic water in the shallow marine conditions. Isolated carbonate platforms commonly developed on the Saharan platform and many were not drowned during the C/T transgression, with carbonate aggradation (‘‘keep-up’’ mechanism) managing to track relative sea-level rise (Lüning et al., 2004; Grosheny et al., 2008). The mechanisms controlling the observed locally distributed organic matter in Errachidia are interpreted to be related not soley to the global marine transgression, but reflects a palaeoenvironmental change caused by the combined effect of eustatic related sea level rise and coeval tectonic subsidence (Grosheny et al., 2008).

Organic matter preservation in marine environments is commonly considered to be controlled by the interplay of primary productivity, preservation conditions and dilution Pedersen and Calvert (1990, AAPG Bulletin) (Pedersen and Calvert, 1990; Sageman et al., 2003; Meyers et al., 2005; Meyers et al., 2012; Tessin et al., 2015). The late Cenomanian sea level rise significantly increased organic matter production on the platforms, with a concomitant reduction in siliciclastic and carbonate dilution, favouring organic matter deposition. This is evidenced by the low detrital-sensitive element concentration (Figure 11), while the increased

productivity and preservation sensitive elements of organic-rich mudstones suggest preservation and productivity are likely to be significant factors responsible for organic matter accumulation in the Errachidia area.

5.3.1. Preservation

Studies from Algeo and Maynard (2004) and Tribovillard et al. (2006) show a covariant relationship between certain sets of trace elements and TOC concentration in different water conditions and a comparable trend is recognised in the Errachidia section (Figure 17). In oxic and dysoxic bottom water conditions, there is no covariance between trace elements and TOC values (Algeo and Maynard, 2004; Tribovillard et al., 2006), and this could be evidenced in the LBL and UBL units. However, the trace elements are extremely concentrated and show positive correlation with TOC values in anoxic water conditions, and this correlation could be recognised in the OM-rich black mudstone of the lower and upper MFL unit. This is consistent with the Ni/Co-U/Th cross-plot (Figure 13). In organic-rich mudstone intervals in the middle MFL unit, element concentration exhibits two distinct patterns: 1) V, Zn, Mo and U show a significant increase in spite there being no significant TOC increase. These elements are known to have a strong euxinic affinity; 2) Ni, Cu, and Co, which are considered as showing organic matter affinity, are only weakly enriched (Algeo and Maynard, 2004; Tribovillard et al., 2006). It has been widely reported that the precipitation of V, Zn, Mo and U can be strongly enhanced in sulfidic euxinic facies (Algeo and Maynard, 2004; Tribovillard et al., 2006). Accordingly, we conclude tentatively that the middle part of the MFL unit was developed, at least periodically, in euxinic water conditions.

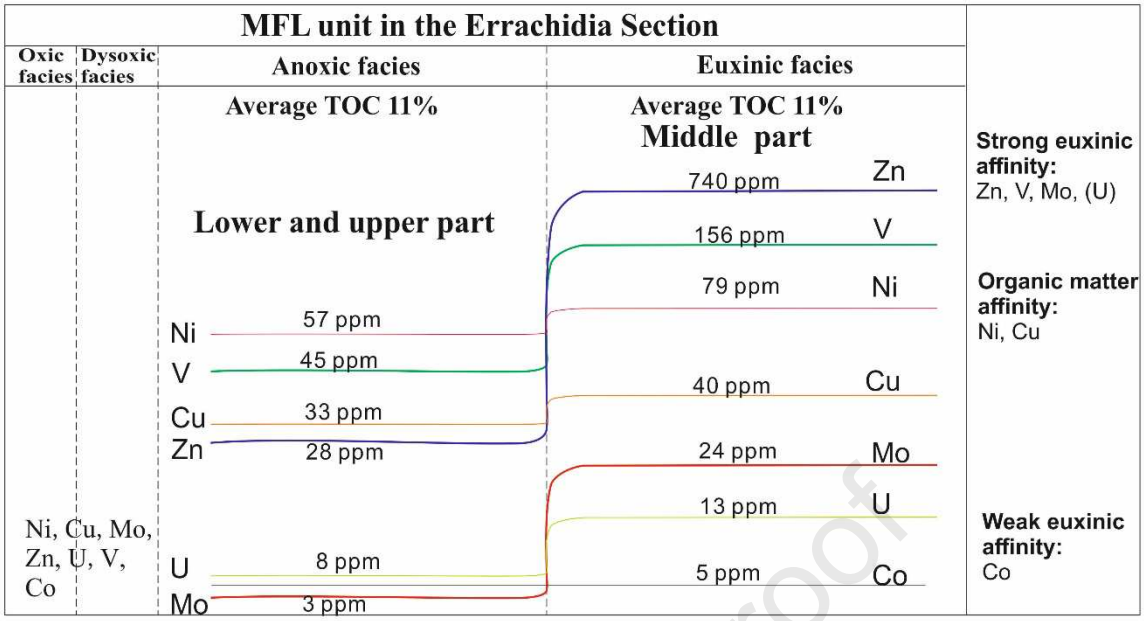

Figure 17. Schematic diagram of the relationship between the enrichment of Zn, V, Ni, Cu, Mo, U and Co, and redox facies in the MFL unit of the Errachidia section (Modified after Algeo and Maynard, 2004; Tribovillard et al., 2006).

The major late Cenomanian and early Turonian marine transgression into this basin might intensify the water column stratification (Arthur and Sageman, 2005; Jenkyns, 2010), favouring the development of anoxic/euxinic conditions in this area. However, the onset of organic matter accumulation in the late Cenomanian is accompanied by poor/moderate redox-sensitive element concentrations (such as V and Mo), although significant productivity-sensitive element enrichment (Ni and Cu) (Figure 11) is observed. Moreover, the relationship between the redox-sensitive elements (V, Mo and U) and TOC values (R^2= 0.29, 0.23, 0.28 separately) presents a weaker correlation compared with the covariant between productivity-sensitive elements (Ni, Zn and Cu) and TOC (R^2=0.70, 0.14 and 0.49). This can especially be distinguished at the onset of anoxic water conditions. This suggests preservation was perhaps not as important a factor as productivity.

5.3.2. Productivity

In the Errachidia section, the productivity-sensitive element concentrations (P, Ni, Zn and Cu) are extremely high in the MFL unit compared to the LBL and UBL units. In the Tadighoust and Goulmima sections, these elements also show a salient enhancement in the MFL unit compared with other units, despite being much weaker than in the Errachidia section (Figure 11). This suggests increased productivity across the whole area in the MFL, with extremely high productivity in the Errachidia area.

During the late Cenomanian/early Turonian, nutrient-rich upwelling water masses are widely recorded along the Atlantic and Tethys Ocean coastlines (Arthur and Schlanger, 1979; Schlanger et al., 1987; Lüning et al., 2004; Kolonic et al., 2005; Keller, 2008; Trabucho Alexandre et al., 2010; Lowery et al., 2017). Extensive upwelling along the coastline was conducive to water mass and nutrient exchange between adjacent basins. Increased silica (quartz dominant) content is recorded in the organic-rich mudstones, and the absence of siliceous fossils (such as radiolarian) suggests this has a mainly continental origin.

The dominance of kaolinite and absence of smectite in the C/T sediments (Lebedel et al., 2013) indicates a warm and humid paleoclimate (Deconinck and Chamley, 1995; Adatte et al., 2002), which could have intensified continental weathering of North-West African margin through geochemical and physical processes (Jenkyns, 2010; Monteiro et al., 2012; Von Strandmann et al., 2013). Moreover, the recognised regional/global sea level transgression could also bring some nutrients into the marine environment though flooding of the continental margin. Therefore, global enhanced productivity could be explained by the increased rate of nutrient supply owing to enhanced continental weathering during the C/T interval (Jenkyns, 2010; Monteiro et al., 2012). However, only moderate concentrations of detrital influx sensitive elements (Figure 11) are recorded during the organic-rich mudstone

763 deposition in Errachidia area, which seem insufficient to explain the high productivity.
764 Moreover, the interval with the highest productivity (highest recorded TOCs) is not coeval
765 with the strongest detrital input. This suggests that terrigenous input might not be the only
766 nutrient source for the extremely high trace elements concentration during the organic matter
767 preservation.

768 The presence of organic-poor limestone/organic-rich mudstones couplets in the MFL unit
769 indicate the absence of long-term anoxic/euxinic bottom water conditions from latest
770 Cenomanian to earliest Turonian. Dysoxic/anoxic fluctuation is commonly recognised in
771 shallow marine environments and has been interpreted as being driven by the periodical
772 thermocline (Tyson and Pearson, 1991; Sageman et al., 2003), attributed to climate and/or
773 productivity cycles (Elderbak and Leckie, 2016). This is interpreted to reflect changes in
774 stratification-mixing associated with periodic upwelling of bottom water nutrients (Sageman
775 et al., 2003; Jenkyns, 2010), that stimulated surface plankton productivity.

776 Based on the above observations, we conclude that the onset of OM-rich black mudstone
777 deposition was primarily triggered by an increase in productivity, associated with increased
778 continental weathering and an accelerated hydrological cycle. The upwelling and increased
779 surface productivity could drive the development of an oxygen minimum zone (OMZ) in the
780 water column (Kuypers et al., 2002; Takashima et al., 2006; Lowery et al., 2018), and
781 accelerate the development of anoxic/euxinic bottom water conditions.

782 Ultimately, the interplay between high productivity, lack of dilution and preservation and
783 presence of anoxic/euxinic bottom water conditions facilitated the preservation of
784 considerable amounts of OM in the Errachidia area.

6. Conclusions

1) High-resolution logging of 7 outcrops near to Errachidia in Morocco has allowed twelve lithofacies to be identified, recording depositional in a shallow marine environment.
2) The location of the C/T boundary within the studied sections has been redefined, based on new biostratigraphic (planktic foraminifera and ammonites) and carbon isotope stratigraphic analysis. This moves the boundary up section from previous work.
3) No organic-rich mudstones have been recorded in the early Upper Cenomanian. OM-poor carbonates are the dominant deposits in the studied basin on the platforms. The organic-rich black mudstones only developed in the Errachidia area, deposited from the latest Cenomanian to early Turonian, an interval that mostly postdates the OAE2 event as defined by carbon isotopic stratigraphy.
4) Trace and major elements analysis suggest oxic water conditions and low productivity prevailed in the early part of the Upper Cenomanian, with significant environmental change occuring in the latest Cenomanian to early Turonian, leading high productivity and anoxic/euxinic water conditions in the Errachidia area. However, conditions continued to be predominantly oxic or slightly dysoxic on the shallow ramp, with only marginally enhanced productivity over most areas, preventing OM preservation. The interplay of high productivity and anoxic/euxinic water conditions facilitated the considerable organic matter preservation in the Errachidia section. By the late early Turonian, a subsequent regression resulted in a shift back to dominantly bioclastic-rich limestones deposited across the basin, in a middle ramp environment.
5) The late Cenomanian/early Turonian marine transgression is interpreted as a regional/global event, which has also controlled deposition of OM-rich black mudstones in more distant Tethyan basins.

7. Acknowledgements

The authors gratefully acknowledge the sponsoring companies of North Africa Research Group and the Office National des Hydrocarbures et des Mines (ONHYM) for their financial and scientific support. We wish to thank: Dr. Youssi Mohamed Zakaria (ONHYM, Rabat) and David Taylor (University of Manchester) for their help and support during the fieldwork; Dr. Alastair Bewsher and Dr. Paul Lythgoe (University of Manchester) for the XRF analysis; Mr. Steve Stockley (University of Manchester) for the powder samples preparation; Dr. Stephen Crowley (University of Liverpool) for the stable carbon and oxygen isotope analysis; Dr. John Waters (University of Manchester) for the XRD training; and Dr Mike Simmons from Halliburton for the planktonic foraminifera analysis. We also appreciate the help from Professor Cathy Hollis (University of Manchester) and Professor Gregory Price (University of Plymouth) for their critical suggestions to an earlier version of this contribution.

8. References

Adatte, T., Keller, G., Stinnesbeck, W., 2002. Late Cretaceous to early Paleocene climate and sea-level fluctuations: the Tunisian record. Palaeogeography, Palaeoclimatology, Palaeoecology 178, 165-196.

Aguado, R., Reolid, M., Molina, E., 2016. Response of calcareous nannoplankton to the Late Cretaceous oceanic anoxic event 2 at Oued Bahloul (Central Tunisia). Palaeogeography, Palaeoclimatology, Palaeoecology 459, 289-305.

Algeo, T.J., Maynard, J.B., 2004. Trace-element behavior and redox facies in core shales of Upper Pennsylvanian Kansas-type cyclothems. Chemical Geology 206, 289-318.

Algeo, T.J., Tribovillard, N., 2009. Environmental analysis of paleoceanographic systems based on molybdenum–uranium covariation. Chemical Geology 268, 211-225.

Ambroggi, R., Choubert, G., 1952. Anti-Atlas et vallée du Draa. Hydrogéologie du Maroc. 19ème Congrès international de Géologie, Alger. Notes et Mémoires du Service Géologique du Maroc 97, 323-335.

Andreu, B., Lebedel, V., Wallez, M.-J., Lézin, C., Ettachfini, E.M., 2013. The upper Cenomanian–lower Turonian carbonate platform of the Preafrican Trough, Morocco:

838 Biostratigraphic, paleoecological and paleobiogeographical distribution of ostracods.
839 Cretaceous Research 45, 216-246.

840 Arthur, M.A., Sageman, B.B., 2005. Sea-level control on source-rock development:
841 perspectives from the Holocene Black Sea, the mid-Cretaceous Western Interior Basin of
842 North America, and the Late Devonian Appalachian Basin. Society for Sedimentary Geology
843 82, 35-59.

844 Arthur, M.A., Schlanger, S.O., 1979. Cretaceous "oceanic anoxic events" as causal factors in
845 development of reef-reservoired giant oil fields. AAPG Bulletin 63, 870-885.

846 Basse, E., Choubert, G., 1959. Les faunes d'ammonites du «Cénomano-Turonien» de la
847 partie orientale du domaine atlasique marocain et de ses annexes sahariennes.-[In:] Kellum
848 LB. El Sistema Cretácico2, 59-81.

849 Benadla, M., Reolid, M., Marok, A., El Kamali, N., 2018. The Cenomanian–Turonian
850 transition in the carbonate platform facies of the Western Saharan Atlas (Rhoundjaïa
851 Formation, Algeria). Journal of Iberian Geology 44, 405-429.

852 Benyoucef, M., Mebarki, K., Ferré, B., Adaci, M., Bulot, L.G., Desmares, D., Villier, L.,
853 Bensalah, M., Frau, C., Ifrim, C., 2017. Litho-and biostratigraphy, facies patterns and
854 depositional sequences of the Cenomanian-Turonian deposits in the Ksour Mountains
855 (Saharan Atlas, Algeria). Cretaceous Research 78, 34-55.

856 Benyoucef, M., Meister, C., Mebarki, K., Läng, É., Adaci, M., Cavin, L., Malti, F.-Z., Zaoui,
857 D., Cherif, A., Bensalah, M., 2016. Évolution lithostratigraphique, paléoenvironnementale et
858 séquentielle du Cénomanien-Turonien inférieur dans la région du Guir (Ouest algérien).
859 Carnets de Géologie 16, 271-295.

860 Brumsack, H.-J., 1989. Geochemistry of recent TOC-rich sediments from the Gulf of
861 California and the Black Sea. Geologische Rundschau 78, 851-882.

862 Brumsack, H.-J., 2006. The trace metal content of recent organic carbon-rich sediments:
863 implications for Cretaceous black shale formation. Palaeogeography, Palaeoclimatology,
864 Palaeoecology 232, 344-361.

865 Busson, G., Dhondt, A., Amédro, F., Néraudeau, D., Cornée, A., 1999. La grande
866 transgression du Cénomanien supérieur-Turonien inférieur sur la Hamada de Tinrhert (Sahara
867 algérien): datations biostratigraphiques, environnement de dépôt et comparaison d'un témoin
868 épicratonique avec les séries contemporaines à matière organique du Maghreb. Cretaceous
869 Research 20, 29-46.

870 Calvert, S., Pedersen, T., 1993. Geochemistry of recent oxic and anoxic marine sediments:
871 implications for the geological record. Marine Geology 113, 67-88.

872 Caron, M., Dall'Agnolo, S., Accarie, H., Barrera, E., Kauffman, E.G., Amédro, F.,
873 Robaszynski, F., 2006. High-resolution stratigraphy of the Cenomanian–Turonian boundary
874 interval at Pueblo (USA) and wadi Bahloul (Tunisia): stable isotope and bio-events
875 correlation. Geobios 39, 171-200.

876 Courville, P., 1993. Les formations marines et les faunes d'ammonites cénomaniennes et
877 turoniennes(crétacé supérieur) dans le fossé de la Bénoué(Nigéria). Impact des facteurs
878 locaux et globaux sur les échanges fauniques à l'interface Téthys-Atlantique Sud, Thèse de
879 Doctorat de l'Université de Bourgogne, p. 350 p.

880 Deconinck, J., Chamley, H., 1995. Diversity of smectite origins in Late Cretaceous
881 sediments: example of chalks from northern France. Clay Minerals 30, 365-379.

882 Dickson, A.J., Jenkyns, H.C., Porcelli, D., van den Boorn, S., Idiz, E., 2016. Basin-scale
883 controls on the molybdenum-isotope composition of seawater during Oceanic Anoxic Event
884 2 (Late Cretaceous). Geochimica et Cosmochimica Acta 178, 291-306.

885 Du Vivier, A.D., Selby, D., Sageman, B.B., Jarvis, I., Gröcke, D.R., Voigt, S., 2014. Marine
886 187Os/188Os isotope stratigraphy reveals the interaction of volcanism and ocean circulation
887 during Oceanic Anoxic Event 2. Earth and Planetary Science Letters 389, 23-33.

888 Dubar, G., 1948. La Faune Domérienne du Jebel Bou-Dahar. Notes et Mémoires du Service
889 Géologique Maroc. Notes Mém. Serv. géol. Maroc 68, 248.

890 El-Sabbagh, A., Tantawy, A.A., Keller, G., Khozyem, H., Spangenberg, J., Adatte, T.,
891 Gertsch, B., 2011. Stratigraphy of the Cenomanian–Turonian Oceanic Anoxic Event OAE2
892 in shallow shelf sequences of NE Egypt. Cretaceous Research 32, 705-722.

893 Elderbak, K., Leckie, R.M., 2016. Paleocirculation and foraminiferal assemblages of the
894 Cenomanian–Turonian Bridge Creek Limestone bedding couplets: productivity vs. dilution
895 during OAE2. Cretaceous Research 60, 52-77.

896 Elrick, M., Molina-Garza, R., Duncan, R., Snow, L., 2009. C-isotope stratigraphy and
897 paleoenvironmental changes across OAE2 (mid-Cretaceous) from shallow-water platform
898 carbonates of southern Mexico. Earth and Planetary Science Letters 277, 295-306.

899 Ettachfini, E.M., Andreu, B., 2004. Le Cénomanien et le Turonien de la Plate-forme
900 Préafricaine du Maroc. Cretaceous Research 25, 277-302.

901 Ettachfini, E.M., Souhel, A., Andreu, B., Caron, M., 2005. La limite Cénomanien-Turonien
902 dans le Haut Atlas central, Maroc. Geobios 38, 57-68.

903 Falzoni, F., Petrizzo, M.R., Caron, M., Leckie, R.M., Elderbak, K., 2018. Age and
904 synchronicity of planktonic foraminiferal bioevents across the Cenomanian–Turonian
905 boundary interval (Late Cretaceous). Newsletters on Stratigraphy 51, 343-380.

906 Ferré, B., Mebarki, K., Benyoucef, M., Villier, L., Bulot, L.G., Desmares, D., Benachour,
907 H.B., Marie, L., Sauvagnat, J., Bensalah, M., 2017. Roveacrinids (Crinoidea, Roveacrinida)
908 from the Cenomanian-Turonian of southwest Algeria (Saharan Atlas and Guir Basin),
909 Annales de Paléontologie. Elsevier, pp. 185-196.

910 Fleurance, S., Cuney, M., Malartre, F., Reyx, J., 2013. Origin of the extreme polymetallic
911 enrichment (Cd, Cr, Mo, Ni, U, V, Zn) of the Late Cretaceous–Early Tertiary Belqa Group,
912 central Jordan. Palaeogeography, Palaeoclimatology, Palaeoecology 369, 201-219.

913 Friedrich, O., Norris, R.D., Erbacher, J., 2012. Evolution of middle to Late Cretaceous
914 oceans—a 55 my record of Earth's temperature and carbon cycle. Geology 40, 107-110.

915 Gale, A.S., Kennedy, W.J., Martill, D., 2017. Mosasauroid predation on an ammonite–
916 Pseudaspidoceras–from the Early Turonian of south-eastern Morocco. Acta Geologica
917 Polonica 67, 31-46.

918 Gertsch, B., Keller, G., Adatte, T., Berner, Z., Kassab, A., Tantawy, A., El-Sabbagh, A.,
919 Stueben, D., 2010. Cenomanian–Turonian transition in a shallow water sequence of the Sinai,
920 Egypt. International Journal of Earth Sciences 99, 165-182.

921 Grosheny, D., Chikhi-Aouimeur, F., Ferry, S., Benkherouf-Kechid, F., Jati, M., Atrops, F.,
922 Redjimi-Bourouiba, W., 2008. The Upper Cenomanian-Turonian (Upper Cretaceous) of the
923 Saharan Atlas (Algeria). Bulletin de la Société géologique de France 179, 593-603.

924 Grosheny, D., Ferry, S., Jati, M., Ouaja, M., Bensalah, M., Atrops, F., Chikhi-Aouimeur, F.,
925 Benkerouf-Kechid, F., Negra, H., Salem, H.A., 2013. The Cenomanian–Turonian boundary
926 on the Saharan Platform (Tunisia and Algeria). Cretaceous Research 42, 66-84.

927 Haq, B.U., 2014. Cretaceous eustasy revisited. Global and Planetary Change 113, 44-58.

928 Hernández-Romano, U., Aguilera-Franco, N., Martínez-Medrano, M.n., Barceló-Duarte, J.,
929 1997. Guerrero-Morelos Platform drowning at the Cenomanian–Turonian boundary,
930 Huitziltepec area, Guerrero State, southern Mexico. Cretaceous Research 18, 661-686.

931 HUA□ZHANG, P., 1990. Late Cretaceous gastropod dominated communities of the western
932 Tarim Basin, southern Xinjiang, China. Lethaia 23, 273-289.

933 Jarvis, I., Lignum, J.S., Gröcke, D.R., Jenkyns, H.C., Pearce, M.A., 2011. Black shale
934 deposition, atmospheric CO2 drawdown, and cooling during the Cenomanian□Turonian
935 Oceanic Anoxic Event. Paleoceanography 26, PA3201.

936 Jarvis, I., Trabucho□Alexandre, J., Gröcke, D.R., Uličný, D., Laurin, J., 2015.
937 Intercontinental correlation of organic carbon and carbonate stable isotope records: evidence
938 of climate and sea□level change during the Turonian (Cretaceous). The Depositional Record
939 1, 53-90.

940 Jenkyns, H., 1980. Cretaceous anoxic events: from continents to oceans. Journal of the
941 Geological Society 137, 171-188.

942 Jenkyns, H.C., 2010. Geochemistry of oceanic anoxic events. Geochemistry, Geophysics,
943 Geosystems 11, 1– 30.

944 Jones, B., Manning, D.A., 1994. Comparison of geochemical indices used for the
945 interpretation of palaeoredox conditions in ancient mudstones. Chemical Geology 111, 111-
946 129.

947 Keller, G., 2008. Cretaceous climate, volcanism, impacts, and biotic effects. Cretaceous
948 Research 29, 754-771.

949 Keller, G., Berner, Z., Adatte, T., Stueben, D., 2004. Cenomanian–Turonian and δ13C, and
950 δ18O, sea level and salinity variations at Pueblo, Colorado. Palaeogeography,
951 Palaeoclimatology, Palaeoecology 211, 19-43.

952 Kennedy, W., Walaszczyk, I., Cobban, W., 2005. The global boundary stratotype section and
953 point for the base of the Turonian stage of the Cretaceous: Pueblo, Colorado, USA. Episodes-
954 Newsmagazine of the International Union of Geological Sciences 28, 93-104.

955 Kennedy, W., Wright, C., Hancock, J., 1987. Basal Turonian ammonites from west Texas.
956 Palaeontology 30, 27-74.

957 Kennedy, W.J., Gale, A.S., Ward, D.J., Underwood, C.J., 2008. Early Turonian ammonites
958 from Goulmima, southern Morocco. Bull Institut Roy Sci Natur Belg Sci Terre 78, 149-177.

959 Kolonic, S., Wagner, T., Forster, A., Sinninghe Damsté, J.S., Walsworth□Bell, B., Erba, E.,
960 Turgeon, S., Brumsack, H.J., Chellai, E.H., Tsikos, H., 2005. Black shale deposition on the
961 northwest African Shelf during the Cenomanian/Turonian oceanic anoxic event: Climate
962 coupling and global organic carbon burial. Paleoceanography 20, PA1006.

963 Korbar, T., Glumac, B., Tešović, B.C., Cadieux, S.B., 2012. Response of a carbonate
964 platform to the Cenomanian–Turonian Drowning and OAE 2: a case study from the Adriatic
965 Platform (Dalmatia, Croatia) Journal of Sedimentary Research 82, 163-176.

966 Košťák, M., Čech, S., Uličný, D., Sklenář, J., Ekrt, B., Mazuch, M., 2018. Ammonites,
967 inoceramids and stable carbon isotopes of the Cenomanian–Turonian OAE2 interval in
968 central Europe: Pecínov quarry, Bohemian Cretaceous Basin (Czech Republic). Cretaceous
969 Research 87, 150-173.

970 Kuhnt, W., Holbourn, A.E., Beil, S., Aquit, M., Krawczyk, T., Flögel, S., Chellai, E.H.,
971 Jabour, H., 2017. Unraveling the onset of Cretaceous Oceanic Anoxic Event 2 in an extended
972 sediment archive from the Tarfaya□Laayoune Basin, Morocco. Paleoceanography 32, 923-
973 946.

974 Kuhnt, W., Luderer, F., Nederbragt, S., Thurow, J., Wagner, T., 2005. Orbital-scale record of
975 the late Cenomanian–Turonian oceanic anoxic event (OAE-2) in the Tarfaya Basin
976 (Morocco). International Journal of Earth Sciences 94, 147-159.

977 Kuypers, M.M., Pancost, R.D., Nijenhuis, I.A., Sinninghe Damsté, J.S., 2002. Enhanced
978 productivity led to increased organic carbon burial in the euxinic North Atlantic basin during
979 the late Cenomanian oceanic anoxic event. Paleoceanography 17, 3-1-3-13.

980 Lebedel, V., Lézin, C., Andreu, B., Wallez, M.-J., Ettachfini, E.M., Riquier, L., 2013.
981 Geochemical and palaeoecological record of the Cenomanian–Turonian Anoxic Event in the
982 carbonate platform of the Preafrican Trough, Morocco. Palaeogeography, Palaeoclimatology,
983 Palaeoecology 369, 79-98.

984 Leckie, R.M., 1985. Foraninifera of the Cenomanian-Turonian Boundary Interval, Greenhorn
985 Formation, Rock Canyon Anticline, Pueblo, Colorado. In: Pratt, L.M.,Kauffman, E.G., Zelt,
986 F.B. (Eds.), Fine-Grained Deposits and Biofacies of the CretaceousWestern Interior Seaway:

987 Evidence of Cyclic Sedimentary Processes. Society of Economic Paleontologists and
988 Mineralogists Field Trip Guidebook, p. 139-149.

989 Leckie, R.M., Yuretich, R.F., West, O.L., Finkelstein, D., Schmidt, M., 1998.
990 Paleoceanography of the southwestern Western Interior Sea during the time of the
991 Cenomanian-Turonian boundary (Late Cretaceous). In: Dean, W.E., Arthur, M.A.(Eds.),
992 Stratigraphy and Paleoenvironments of the Cretaceous Western Interior Seaway, U.S.A.
993 Society Economic Paleontologists and Mineralogists Concepts inSedimentology and
994 Paleontology, Tulsa, 101-126.

995 Lézin, C., Andreu, B., Ettachfini, E.M., Wallez, M.-J., Lebedel, V., Meister, C., 2012. The
996 upper Cenomanian–lower Turonian of the Preafrican Trough, Morocco. Sedimentary
997 Geology 245, 1-16.

998 Lowery, C.M., Corbett, M.J., Leckie, R.M., Watkins, D., Romero, A.M., Pramudito, A.,
999 2014. Foraminiferal and nannofossil paleoecology and paleoceanography of the
1000 Cenomanian–Turonian Eagle Ford Shale of southern Texas. Palaeogeography,
1001 Palaeoclimatology, Palaeoecology 413, 49-65.

1002 Lowery, C.M., Cunningham, R., Barrie, C.D., Bralower, T., Snedden, J.W., 2017. The
1003 northern Gulf of Mexico during OAE2 and the relationship between water depth and black
1004 shale development. Paleoceanography 32, 1316-1335.

1005 Lowery, C.M., Leckie, R.M., Bryant, R., Elderbak, K., Parker, A., Polyak, D.E., Schmidt, M.,
1006 Snoeyenbos-West, O., Sterzinar, E., 2018. The Late Cretaceous Western Interior Seaway as a
1007 model for oxygenation change in epicontinental restricted basins. Earth-Science Reviews
1008 177, 545-564.

1009 Lüning, S., Kolonic, S., Belhadj, E., Belhadj, Z., Cota, L., Barić, G., Wagner, T., 2004.
1010 Integrated depositional model for the Cenomanian–Turonian organic-rich strata in North
1011 Africa. Earth-Science Reviews 64, 51-117.

1012 McCrea, J.M., 1950. On the isotopic chemistry of carbonates and a paleotemperature scale.
1013 The Journal of Chemical Physics 18, 849-857.

1014 Meister, C., Piuz, A., 2013. Late Cenomanian–Early Turonian ammonites of the southern
1015 Tethys margin from Morocco to Oman: biostratigraphy, paleobiogeography and morphology.
1016 Cretaceous Research 44, 83-103.

1017 Meister, C., Piuz, A., Cavin, L., Boudad, L., Bacchia, F., Ettachfini, E.M., Benyoucef, M.,
1018 2017. Late Cretaceous (Cenomanian-Turonian) ammonites from southern Morocco and south
1019 western Algeria. Arabian Journal of Geosciences 10, 1.

1020 Meister, C., Rhalmi, M., 2002. Quelques ammonites du Cénomanien-Turonien de la région
1021 d'Errachidia-Boudnid-Erfoud (partie méridionale du Haut Atlas Central, Maroc). Revue de
1022 Paléobiologie 21, 759-779.

1023 Meyers, S.R., Sageman, B.B., Arthur, M.A., 2012. Obliquity forcing of organic matter
1024 accumulation during Oceanic Anoxic Event 2. Paleoceanography 27, PA3212.

1025 Meyers, S.R., Sageman, B.B., Lyons, T.W., 2005. Organic carbon burial rate and the
1026 molybdenum proxy: Theoretical framework and application to Cenomanian□Turonian
1027 oceanic anoxic event 2. Paleoceanography 20.

1028 Monteiro, F., Pancost, R., Ridgwell, A., Donnadieu, Y., 2012. Nutrients as the dominant
1029 control on the spread of anoxia and euxinia across the Cenomanian□Turonian oceanic anoxic
1030 event (OAE2): Model□data comparison. Paleoceanography 27.

1031 Morford, J.L., Emerson, S., 1999. The geochemistry of redox sensitive trace metals in
1032 sediments. Geochimica et Cosmochimica Acta 63, 1735-1750.

1033 Núñez-Useche, F., Canet, C., Barragán, R., Alfonso, P., 2016. Bioevents and redox
1034 conditions around the Cenomanian–Turonian anoxic event in Central Mexico.
1035 Palaeogeography, Palaeoclimatology, Palaeoecology 449, 205-226.

1036 Omana, L., Doncel, R.L., Torres, J.R., Alencaster, G., 2012. Biostratigraphy and
1037 paleoenvironment of the Cenomanian/Turonian boundary interval based on foraminifera from
1038 W Valles-San Luis Potosí Platform, Mexico. Micropaleontology, 457-485.

1039 Pedersen, T., Calvert, S., 1990. Anoxia vs. productivity: what controls the formation of
1040 organic-carbon-rich sediments and sedimentary rocks? AAPG bulletin 74, 454-466.

1041 Pratt, L., Threlkeld, C., 1984. Stratigraphic significance of 13C/12C ratios in mid-Cretaceous
1042 rocks of the Western Interior, USA.

1043 Reolid, M., Sánchez-Quiñónez, C., Alegret, L., Molina, E., 2015. Palaeoenvironmental
1044 turnover across the Cenomanian-Turonian transition in Oued Bahloul, Tunisia: foraminifera
1045 and geochemical proxies. Palaeogeography, Palaeoclimatology, Palaeoecology 417, 491-510.

1046 Robaszynski, F., Zagrarni, M.F., Caron, M., Amédro, F., 2010. The global bio-events at the
1047 Cenomanian-Turonian transition in the reduced Bahloul Formation of Bou Ghanem (central
1048 Tunisia). Cretaceous Research 31, 1-15.

1049 Sageman, B.B., Bina, C.R., 1997. Diversity and species abundance patterns in Late
1050 Cenomanian black shale biofacies, Western Interior, US. Palaios 12, 449-466.

1051 Sageman, B.B., Meyers, S.R., Arthur, M.A., 2006. Orbital time scale and new C-isotope
1052 record for Cenomanian-Turonian boundary stratotype. Geology 34, 125-128.

1053 Sageman, B.B., Murphy, A.E., Werne, J.P., Ver Straeten, C.A., Hollander, D.J., Lyons, T.W.,
1054 2003. A tale of shales: the relative roles of production, decomposition, and dilution in the
1055 accumulation of organic-rich strata, Middle–Upper Devonian, Appalachian basin. Chemical
1056 Geology 195, 229-273.

1057 Sandoval, J., Tavera, J.M., Aoutem, M., Ettachfini, M., 2008. Barremian ammonite faunas
1058 from the western High Atlas, Morocco–biostratigraphy and palaeobiogeography. Cretaceous
1059 Research 29, 9-26.

1060 Schlanger, S., Arthur, M., Jenkyns, H., Scholle, P., 1987. The Cenomanian-Turonian Oceanic
1061 Anoxic Event, I. Stratigraphy and distribution of organic carbon-rich beds and the marine
1062 δ13C excursion. Geological Society, London, Special Publications 26, 371-399.

1063 Schlanger, S., Jenkyns, H., 1976. Cretaceous oceanic anoxic events: causes and
1064 consequences. Netherlands Journal of Geosciences/Geologie en Mijnbouw 55, 3-4.

1065 Scholle, P.A., Arthur, M.A., 1980. Carbon isotope fluctuations in Cretaceous pelagic
1066 limestones: potential stratigraphic and petroleum exploration tool. AAPG Bulletin 64, 67-87.

1067 Sloss, L., 1963. Sequences in the cratonic interior of North America. Geological Society of
1068 America Bulletin 74, 93-114.

1069 Swart, P.K., Burns, S., Leder, J., 1991. Fractionation of the stable isotopes of oxygen and
1070 carbon in carbon dioxide during the reaction of calcite with phosphoric acid as a function of
1071 temperature and technique. Chemical Geology: Isotope Geoscience section 86, 89-96.

1072 Takashima, R., Nishi, H., Huber, B.T., Leckie, R.M., 2006. Greenhouse world and the
1073 Mesozoic ocean. Oceanography 19, 82-92.

1074 Tessin, A., Hendy, I., Sheldon, N., Sageman, B., 2015. Redox□controlled preservation of
1075 organic matter during “OAE 3” within the Western Interior Seaway. Paleoceanography and
1076 Paleoclimatology 30, 702-717.

1077 Trabucho Alexandre, J., Tuenter, E., Henstra, G.A., van der Zwan, K.J., van de Wal, R.S.,
1078 Dijkstra, H.A., de Boer, P.L., 2010. The mid□Cretaceous North Atlantic nutrient trap: black
1079 shales and OAEs. Paleoceanography 25.

1080 Tribovillard, N., Algeo, T., Baudin, F., Riboulleau, A., 2012. Analysis of marine
1081 environmental conditions based onmolybdenum–uranium covariation—Applications to
1082 Mesozoic paleoceanography. Chemical Geology 324, 46-58.

1083 Tribovillard, N., Algeo, T.J., Lyons, T., Riboulleau, A., 2006. Trace metals as paleoredox and
1084 paleoproductivity proxies: an update. Chemical Geology 232, 12-32.

1085 Tsikos, H., Jenkyns, H., Walsworth-Bell, B., Petrizzo, M., Forster, A., Kolonic, S., Erba, E.,
1086 Silva, I.P., Baas, M., Wagner, T., 2004. Carbon-isotope stratigraphy recorded by the
1087 Cenomanian–Turonian Oceanic Anoxic Event: correlation and implications based on three
1088 key localities. Journal of the Geological Society 161, 711-719.

1089 Turekian, K.K., Wedepohl, K.H., 1961. Distribution of the elements in some major units of
1090 the earth's crust. Geological Society of America Bulletin 72, 175-192.

1091 Tyson, R.V., Pearson, T.H., 1991. Modern and ancient continental shelf anoxia: an overview.
1092 Geological Society, London, Special Publications 58, 1-24.

1093 Van der Weijden, C.H., 2002. Pitfalls of normalization of marine geochemical data using a
1094 common divisor. Marine Geology 184, 167-187.

1095 Van Helmond, N.A., Sluijs, A., Reichart, G.-J., Damsté, J.S.S., Slomp, C.P., Brinkhuis, H.,
1096 2014. A perturbed hydrological cycle during Oceanic Anoxic Event 2. Geology 42, 123-126.

1097 Von Strandmann, P.A.P., Jenkyns, H.C., Woodfine, R.G., 2013. Lithium isotope evidence for
1098 enhanced weathering during Oceanic Anoxic Event 2. Nature Geoscience 6, 668.

1099 Weaver, P.P., Wynn, R.B., Kenyon, N.H., Evans, J., 2000. Continental margin sedimentation,
1100 with special reference to the north□east Atlantic margin. Sedimentology 47, 239-256.

1101 Wedepohl, K., 1971. Environmental influences on the chemical composition of shales and
1102 clays. Physics and Chemistry of the Earth 8, 307-333.

1103 Wedepohl, K.H., 1995. The composition of the continental crust. Geochimica et
1104 Cosmochimica Acta 59, 1217-1232.

1105 Zagrarni, M.F., Negra, M.H., Hanini, A., 2008. Cenomanian–Turonian facies and sequence
1106 stratigraphy, Bahloul formation, Tunisia. Sedimentary Geology 204, 18-35.

1107 Zouhri, S., Kchikach, A., Saddiqi, O., El Haïmer, F., Baidder, L., Michard, A., 2008. The
1108 cretaceous-tertiary plateaus, Continental Evolution: The Geology of Morocco. Springer, pp.
1109 331-358.

1110

Highlights of the paper:

1. Improve dating of the Cenomanian/Turonian boundary and OAE2 interval in Morocco.
2. First description of C/T OM-rich mudstone deposition in the Pre-African Basin.
3. Reconstruct the paleoenvironments of organic-rich mudstone deposition
4. Investigate the driving factors of C/T OC deposition in the Pre-African Basin

Declaration of interests

☒ The authors declare that they have no known competing financial interests or personal relationships that could have appeared to influence the work reported in this paper.

☐The authors declare the following financial interests/personal relationships which may be considered as potential competing interests: